



# Changes in the impacts of ship emissions on PM<sub>2.5</sub> and its components in China under the staged fuel oil policies

Guangyuan Yu<sup>1,2</sup>, Yan Zhang<sup>1,3,4</sup>, Qian Wang<sup>2</sup>, Zimin Han<sup>1</sup>, Shenglan Jiang<sup>1</sup>, Fan Yang<sup>5</sup>, Xin Yang<sup>6</sup>, and Cheng Huang<sup>2</sup>

<sup>1</sup>Shanghai Key Laboratory of Atmospheric Particle Pollution and Prevention (LAP<sup>3</sup>), National Observations and Research Station for Wetland Ecosystems of the Yangtze Estuary, Department of Environmental Science and Engineering, Fudan University, Shanghai 200438, China

<sup>2</sup>Shanghai Environmental Monitoring Center (SEMC), Shanghai 200235, China

<sup>3</sup>Shanghai Institute of Eco Chongming (SIEC), Shanghai 200062, China

<sup>4</sup>MOE laboratory for National Development and Intelligent Governance, Shanghai institute for energy and carbon neutrality strategy, IRDR ICoE on Risk Interconnectivity and Governance on Weather/Climate Extremes Impact and Public Health, Fudan University, Shanghai 200433, China

<sup>5</sup>Pudong New Area Environmental Monitoring Station, Shanghai 200135, China

<sup>6</sup>Shenzhen Key Laboratory of Precision Measurement and Early Warning Technology for Urban Environmental Health Risks, School of Environmental Science and Engineering, Southern University of Science and Technology, Shenzhen 518055, China

**Correspondence:** Yan Zhang (yan\_zhang@fudan.edu.cn) and Cheng Huang (huangc@saes.sh.cn)

Received: 10 December 2024 – Discussion started: 9 January 2025

Revised: 14 May 2025 – Accepted: 2 June 2025 – Published: 28 August 2025

**Abstract.** The issue of air pollution caused by ship emissions is becoming prominent with the increasing global shipping activities. China has carried out fuel oil policies in three stages in the past few years to meet the requirements of the global low sulfur regulation by the International Maritime Organization (IMO). However, the impacts of staged policies on air quality in China are not sufficiently understood. This study firstly updated the ship emission inventory including PM<sub>2.5</sub> components based on field and on-board measurements under the staged fuel oil policies. Then, the impacts of ship emissions on PM<sub>2.5</sub> and its gas precursors and primary and secondary components in China from 2017 to 2021 were revealed by using the Weather Research and Forecasting (WRF) model and the Community Multiscale Air Quality (CMAQ) model. In the model domain, the 99th percentile of the shipping-related PM<sub>2.5</sub> concentrations was reduced by 19.5 % and then by 35.6 % due to the policy shifts. Ship emissions increased the PM<sub>2.5</sub> concentrations up to 3.8 µg m<sup>-3</sup> in 2017 and 2.6 µg m<sup>-3</sup> in 2021. The areas with high concentration levels widely distributed over offshore waters in 2017 and shrunk to some parts of China's coast in 2021. The contributions of ship emissions to the PM<sub>2.5</sub> concentrations over China's main port cities ranged from 3.0 % to 17.4 % in 2017 and 2.5 % to 10.3 % in 2021. In these cities, the change rates of the concentrations of PM<sub>2.5</sub>, SO<sub>4</sub><sup>2-</sup>, NO<sub>3</sub><sup>-</sup>, NH<sub>4</sub><sup>+</sup>, carbonaceous aerosols, V, and Ni related to ship emissions from 2017 to 2021 were -32.7 %, -74.0 %, +11.0 %, -27.5 %, -76.9 %, -90.3 %, and -38.4 %, respectively. NO<sub>3</sub><sup>-</sup> constituted 54.6 % of the shipping-related PM<sub>2.5</sub> in 2021. Our findings suggest that it is important to consider both transport pathways and secondary aerosol formation mechanisms to combat the PM<sub>2.5</sub> pollution caused by shipping in different regions.

## 1 Introduction

Shipping is the backbone of global trade and transports more than 80 % of global goods. Global shipping activities have increased by  $\sim 20$  % in the past decade and will continue to grow at a rate of  $\sim 2$  % per year in the coming years (UNCTAD, 2023). Meanwhile, heavy fuel oil (HFO) is the most widely used type of fuel for marine vessels. The combustion of HFO can release remarkably higher amounts of sulfur oxides (SO<sub>x</sub>), particulate matter (PM), and trace elements compared to the combustion of lighter oils (Agrawal et al., 2008a; Moldanová et al., 2013; Zhang et al., 2019b). Due to the increasing shipping activities and the low quality of fuel oils, shipping is becoming an important source of air pollution, especially in coastal areas and ports with dense traffic (Dalsøren et al., 2009; Eyring et al., 2010). It is reported that international vessels emitted 9600 kilotons (kt) SO<sub>x</sub>, 17 100 kt NO<sub>x</sub> (nitrogen oxides), and 1351 kt PM<sub>2.5</sub> (PM with a diameter of less than 2.5  $\mu\text{m}$ ) in 2018 (IMO, 2021). In Europe, the maritime transport sector produced 24 % of all NO<sub>x</sub> emissions, 24 % of all SO<sub>x</sub> emissions, and 9 % of all PM<sub>2.5</sub> emissions in 2018, affecting  $\sim 40$  % of Europeans living within 50 km of the sea (EMSA and EEA, 2021). In 2022, China held a national port cargo throughput of 15.68 billion tonnes and was home to 8 of the top 10 ports for cargo throughput and 7 of the top 10 ports for container throughput worldwide (Ministry of Transport of the People's Republic of China, 2023). Tracking ship emissions and their environmental impacts in China is of great significance.

Exposure to high levels of PM<sub>2.5</sub> can increase health problems such as respiratory and cardiovascular diseases. The World Health Organization (WHO) Global Air Quality Guidelines 2021 recommend that annual mean concentrations of PM<sub>2.5</sub> should not exceed 5  $\mu\text{g m}^{-3}$  (WHO, 2021). Studies using chemical transport models (CTMs) have been conducted to simulate the impact of ship emissions on PM<sub>2.5</sub> in the regions with heavy ship traffic. In China, ship emissions increased the annual average PM<sub>2.5</sub> concentrations up to 5.2  $\mu\text{g m}^{-3}$  in 2015, surpassing the limit value recommended by the WHO. In Europe and North America, the increase in PM<sub>2.5</sub> concentrations due to shipping is generally less than 2  $\mu\text{g m}^{-3}$ ; however, its relative contribution is significant, reaching 25 %–50 % along main shipping routes and 12 %–15 % in coastal areas (Aksoyoglu et al., 2016; Tang et al., 2020; Fink et al., 2023a; Golbazi and Archer, 2023). Based on observations, the impact of ship emissions on PM can also be calculated by using source apportionment methods such as receptor models. In China, our previous studies show that ship emissions contribute 1.96  $\mu\text{g m}^{-3}$  (4.23 %) to the ambient PM<sub>2.5</sub> concentration at port and 0.4–3.1  $\mu\text{g m}^{-3}$  (1.3 %–8.8 %) for downtown Shanghai (Zhao et al., 2013; Yu et al., 2021); the fraction of shipping-related particles is 1 %–10 % in port cities (Liu et al., 2017b; Wang et al., 2019; Zhang et al., 2019a; Zhai et al., 2023). Ship emissions contribute to annual mean concentrations of PM<sub>2.5</sub> of 1 %–14 % in Eu-

ropean coastal areas and 3 %–9 % in American coastal areas (Agrawal et al., 2009; Viana et al., 2014; Kotchenruther, 2015; Anastasopoulos et al., 2021).

Shipping-related PM comprises primary particles and secondary products. Ships primarily emit organic carbon (OC), elemental carbon (EC), sulfate, metallic elements, etc., among which OC and sulfate are the main components of primary PM from ships burning HFO (Agrawal et al., 2008b; Lack et al., 2009; Agrawal et al., 2010; Huang et al., 2018a; Yang et al., 2022; Karjalainen et al., 2022). Vanadium (V), nickel (Ni), and the V / Ni ratio are the most commonly used tracers of ship emissions (Agrawal et al., 2009; Moldanová et al., 2009; Celo et al., 2015; Corbin et al., 2018; Yu et al., 2021). Calculating the emissions, the concentrations, and the deposition fluxes of V and Ni from shipping can help us better understand their geochemical cycles. In comparison, sulfate, nitrate, and ammonium (SNA) dominate the shipping-related PM, with their proportion even exceeding 90 % based on modelling research (Lv et al., 2018; Jonson et al., 2020; Fink et al., 2023a; Jang et al., 2023).

Studies have demonstrated that using desulfurized fuel oils can significantly reduce the emissions of various air pollutants, such as SO<sub>x</sub>, PM, OC, heavy metals, and polycyclic aromatic hydrocarbons (PAHs) (Tao et al., 2013; Zetterdahl et al., 2016; Kotchenruther, 2017; Spada et al., 2018; Huang et al., 2018a). To combat the air pollution caused by ship emissions, four emission control areas (ECAs) exist in Europe and North America as of 2011. The sulfur limit for fuel in the ECAs has been restricted to 0.10 % m m<sup>-1</sup> since 1 January 2015. In addition, Tier III, which restricts the NO<sub>x</sub> emission factor to no more than 3.4 g kWh<sup>-1</sup>, entered into force on 1 January 2016 in the ECAs of North America and on 1 January 2021 in the ECAs of Europe. However, the regulations in China are significantly lagging behind those in North America and Europe. The global fuel sulfur limit of 0.50 % (reduced from 3.50 %) has been mandated by the International Maritime Organization (IMO) since 1 January 2020 (IMO Regulation). Before 2017, marine vessels in the region of China generally used HFO with a sulfur content of  $\sim 2.7$  %. To meet the IMO Regulation, the Ministry of Transport of China enacted staged control policies from 2017 to 2020. Ships berthing at the ports in China's Domestic Control Areas (DECAs) were required to use fuel with a sulfur content of no more than 0.50 % (low sulfur fuel oil – LSFO hereafter) after 1 January 2017, known as the DECA 1.0 period. All ships within 12 nautical miles (nm) from the baseline of the territorial sea had to use LSFO after 1 January 2019, which is referred to as the DECA 2.0 period (Liu et al., 2018a; Wang et al., 2021). The inland emission control areas covering the Yangtze River, the Xijiang River, and the Pearl River went into effect after 1 January 2019, where coastal vessels were required to combust LSFO; as of 1 January 2020, both coastal and international vessels have been required to use fuel with a sulfur limit of 0.10 %, called ultra-low sulfur fuel oil (ULSFO). The staged regulations for fuel

sulfur content are summarized in Table S1 in the Supplement. For the NO<sub>x</sub> emission control, newly built ships in China follow the IMO Tier II standard from 2011 that restricts the NO<sub>x</sub> emission factor to no more than 14.4 g kWh<sup>-1</sup>.

The latest published studies have reported the effects of the implementation of the IMO Regulation at global and regional scales. In 2020, relative to 2019, both the sulfur dioxide (SO<sub>2</sub>) and PM<sub>2.5</sub> emissions from shipping were reduced by ~80 % on a global scale (Yi et al., 2025; Wang et al., 2025). In China, the shipping-related PM<sub>2.5</sub> concentrations decreased but mortality increased in port cities from 2016 to 2020 (Luo et al., 2024). In South Korea, the SO<sub>2</sub> and NH<sub>4</sub><sup>+</sup> concentrations and the contributions of shipping to sulfate and OC decreased after 2020 (Song et al., 2022; Jang et al., 2023). However, there are few studies on the impacts of ship emissions on multiple atmospheric pollutants after the implementation of the IMO Regulation based on actual shipping activity data and CTMs (Zhai et al., 2023; Feng et al., 2023). The simulation years of some studies published in the past 2 years from China, Europe, and North America are before the IMO Regulation (Fink et al., 2023b; Fu et al., 2023; Golbazi and Archer, 2023), yet there is little knowledge on the changes in the impacts of ship emissions on air quality under staged fuel oil policies in China since 2017 and on the changes in the specific composition of shipping-related PM. The impacts of meteorology and chemical mechanisms on the PM<sub>2.5</sub> pollution caused by shipping in China are not fully understood. In addition, it was observed in our previous study that the concentrations of V and Ni from shipping decreased significantly and stepwise in China's largest port city from 2017 to 2020. The latest emission inventories of V and Ni from shipping are still not earlier than 2017 and need updating until after 2020 (Zhao et al., 2021; Jiang et al., 2024).

In this study, we updated the ship emission inventory based on the data from the Automatic Identification System (AIS) and simulated the impacts on PM<sub>2.5</sub> in China and its gas precursors (SO<sub>2</sub> and NO<sub>2</sub>) and components from 2017 to 2021 by using the Weather Research and Forecasting (WRF) model and the Community Multiscale Air Quality (CMAQ) model. The emissions of V and Ni from shipping were constrained by the field observational data from our previous study and the results of on-board emission measurements. Based on the simulation results, the spatiotemporal patterns of shipping-related PM<sub>2.5</sub> and of trace elements (V and Ni), secondary inorganic aerosols, and organic aerosols (OAs) were obtained. Meanwhile, the interannual and seasonal variations in the impacts were investigated. Then, we focused on the changes in the impacts due to the IMO Regulation at the port city level. In addition, the roles of the meteorological factors in affecting the seasonal and diurnal patterns of primary PM from shipping over the port cities were discussed.

## 2 Methods

### 2.1 Setup of the WRF/CMAQ

We utilized the CMAQ version 5.4 to simulate the pollutant concentrations and the WRF version 4.1.1 to provide the meteorological input fields for the CMAQ. The WRF physics scheme configuration included the Yonsei University (YSU) scheme for the planetary boundary layer (PBL), the Noah land surface scheme, the Thompson microphysics scheme, the rapid radiative transfer model for general circulation models (RRTMG) for short- and longwave schemes, and the Kain–Fritsch cumulus scheme for cumulus parameterization. A total of 40 vertical layers were set up with the model top pressure at 50 hPa, among which 12 layers were distributed within 1.6 km above the surface. The surface layer thickness was ~50 m. The WRF model was driven by the European Centre for Medium-Range Weather Forecasts (ECMWF) Reanalysis v5 (ERA5) at hourly temporal and 0.25° × 0.25° spatial resolution (Hersbach et al., 2023). To reduce the errors, monthly WRF simulations were divided into six runs, each of which included a 12 h spin-up time. Two nested domain simulations were operated with horizontal resolutions of 27 km × 27 km (d01) and 9 km × 9 km (d02) encompassing eastern Asia and eastern China, respectively. In the CMAQ model, two grids on each WRF lateral boundary were removed; thus there were 161 × 174 and 233 × 215 grids in d01 and d02, respectively. Figure 1 shows the nested domains configured in the CMAQ and the coastal emission control area (CECA) of China covering all the marine waters within 12 nm beyond the territorial baselines.

The CMAQ model was configured to the gas-phase mechanism of Carbon Bond 6 revision 5 (CB6r5) and the aerosol module of AERO7. By modifying the aerosol module and the in-line dust module, two trace elements, V and Ni, were added into the CMAQ as inert aerosol components which only participate in atmospheric physical processes such as diffusion, advection, and deposition. Detailed information on the code modification can be found in the Supplement (Text S1) and in our previous study (Jiang et al., 2024). The initial and boundary conditions for d01 originated from the seasonal average hemispheric CMAQ output from the Community Modeling and Analysis System (CMAS) data repository, while those for d02 were derived from the output data of d01. For the analysis of seasonal variations, the simulations were conducted for January, April, July, and October of 2017 and 2021, representing winter, spring, summer, and autumn, respectively. The annual average was equal to the average of 4 representative months. To study the impacts under staged fuel oil policies and save computing resources, the simulations were operated for each April from 2017 to 2021 based on our previous finding that the impacts of ship emissions in China's coastal areas usually peak in spring (Yu et al., 2021). The spin-up time of each simulation was 5 d. Detailed information on the WRF/CMAQ configuration can

**Table 1.** Details of the WRF/CMAQ configuration.

Simulation period	January, April, July, and October of 2017 and 2021; April of 2018–2020
Grid resolution	27 km × 27 km (d01), 9 km × 9 km (d02)
Vertical layers	40
Surface layer thickness	50 m
Top of model	50 hPa
WRF version 4.1.1	
Grid size	165 (south to north) × 178 (west to east) (d01); 237 × 219 (d02)
Initial/boundary conditions	ECMWF Reanalysis v5 (ERA5), hourly, 0.25° × 0.25°
Microphysics scheme	Thompson
Land surface model	Noah
Planetary boundary layer scheme	Yonsei University (YSU), topo_wind = 2
Cumulus scheme	Kain–Fritsch
Shortwave radiation	Rapid radiative transfer model for general circulation models (RRTMG)
Longwave radiation	RRTMG
Spin-up time	12 h
Number of days per run	6.5*
CMAQ version 5.4	
Grid size	161 × 174 (d01); 233 × 215 (d02)
Initial/boundary conditions	EPA 2017–2018 (d01); output of d01 run (d02)
Gas-phase mechanism	Carbon Bond 6 revision 5 (CB6r5)
Aerosol module	AERO7
Spin-up time	5 d
Number of days per run	36 for January, July, and October; 35 for April

\* For WRF, the last run of April is an exception, with a time length of 5.5 d.

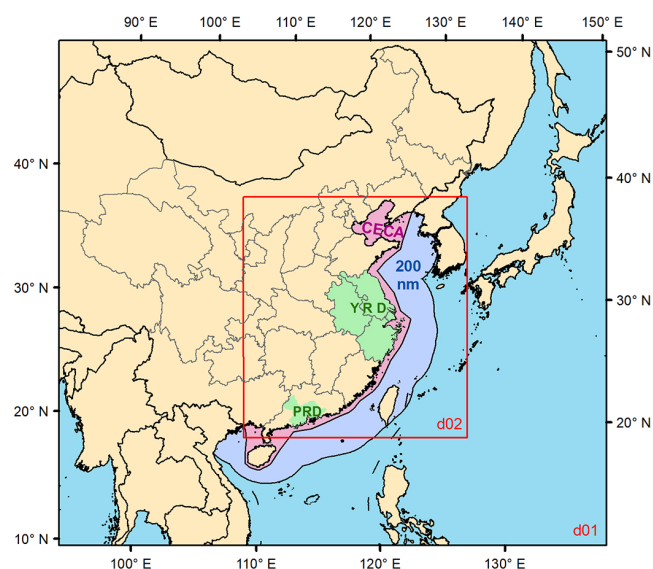


**Figure 1.** Map of the nested domains configured in the CMAQ. The coastal emission control area (CECA) of China is coloured in pink. The border of the area within 200 nautical miles (nm) from the coastline of the Chinese mainland is outlined. The Yangtze River Delta (YRD) and the Pearl River Delta (PRD) are coloured in green.

be seen in Table 1. The impacts of ship emissions were extracted based on the zero-out method, i.e. two runs with and without ship emissions, named the base run and the exship run, respectively, in this study.

## 2.2 Emission data

### 2.2.1 Ship emissions

A bottom-up ship emission model based on the AIS data was used to calculate the emission inventories of SO<sub>2</sub>, NO<sub>x</sub>, carbon monoxide (CO), nonmethane volatile organic compounds (NMVOCs), PM with a diameter less than 10 µm (PM<sub>10</sub>), PM<sub>2.5</sub>, ammonia (NH<sub>3</sub>), V, and Ni. Detailed information on the setup of the ship emission model can be found in the Supplement (Text S2) and in our previous studies (Fan et al., 2016; Feng et al., 2019). In the ship emission model, the power-based emission factors (EFs) under the staged fuel oil policies are categorized by engine type (Table S2).

During the DECA 1.0 period (2017–2018), we adopted the EFs of various species from Fan et al. (2016) and the fourth IMO Greenhouse Gas (GHG) study. The default setting for main engines (MEs), including slow-speed diesel (SSD) and medium-speed diesel (MSD) engines usually installed for large vessels, was high sulfur fuel oil (HSFO) with a sulfur content of ~ 2.7 %. A high-speed diesel engine as a main engine (ME\_HSD) generally used marine diesel oil (MDO)



or marine gas oil (MGO) with a sulfur content of  $\sim 0.1\%$ . An auxiliary engine (AE) was assumed to use LSFO with a sulfur content of  $\sim 0.5\%$ .

During the DECA 2.0 period (2019), the settings remained the same as those during the DECA 1.0 period in the marine areas outside the CECA. In the CECA, the scenario of EF setting for MEs of large vessels was LSFO. For the AE, considering that LSFO is often used by seagoing vessels in addition to ULSFO, we took the mean values of the EFs for LSFO and ULSFO.

After the implementation of the IMO Regulation, the settings in all marine areas followed those in the CECA during the DECA 2.0 period. Over land areas, for the seagoing vessels, the EFs of SO<sub>2</sub> and PM for MEs were scaled by a factor of 0.2 and 0.26 and of 0.315 and 0.391 for AE, respectively, which is due to the implementation of the inland river emission control areas. The EFs of V and Ni for ships navigating in inland waters were lowered by a factor of 10 for the ME due to the non-linearity between the contents of sulfur and trace elements.

In terms of the EFs of V and Ni for marine vessels during the DECA 1.0 period, we used the values reported in the literature listed in Table S3. These values during the DECA 2.0 and after 2020 were reduced corresponding to the change ratios reported in our previous study (Yu et al., 2021). The emission inventories of V and Ni were validated through comparison between simulation results and observational data in Shanghai along with observational data in several coastal cities reported by other studies.

The mapping of PM<sub>2.5</sub> components from shipping to the AERO7 species is shown in Table S4. The mass fractions before the IMO Regulation (2017–2019) and after 2020 were referenced from Huang et al. (2018a) and Yang et al. (2022), respectively. The convert factors of NMVOC emissions from shipping to lumped species in the CB6 mechanism were based on the median volatile organic compound (VOC) profiles from the literature (Table S5) (Agrawal et al., 2008a; Huang et al., 2018b; Zhang et al., 2024). The initial height of ship emissions considering plume rise and diffusion is basically in the range of 20–100 m (Chosson et al., 2008; He et al., 2021; Badeke et al., 2022; Lansø et al., 2023). We allocated 20 % of the seagoing vessel emissions to the surface layer (0–50 m) and 80 % to the second layer (50–109 m), while all the inland ship emissions were assigned in the surface layer (Table S6).

### 2.2.2 Land-based emissions

For land-based anthropogenic emissions, we used the Multi-resolution Emission Inventory for China (MEIC) in 2017–2020 for mainland China and the MIX emission data in 2010 for eastern Asia excluding mainland China (Li et al., 2017; Zheng et al., 2021). The NH<sub>3</sub> emissions in the MEIC were replaced by the PKU-NH<sub>3</sub> inventory in 2017 (Kang et al., 2016). For natural sources, we used the CAMS-GLOB-

BIO v3.1 for monthly global biogenic VOC (BVOC) emissions in 2017–2021 and the biogenic emissions inventory from urban green spaces in China (OUC-BUGS) in 2017–2019 (Sindelarova et al., 2021; Ma et al., 2022). The MEIC, MIX, PKU-NH<sub>3</sub>, and OUC-BUGS inventories were downloaded from the website (<http://meicmodel.org.cn/>, last access: 30 September 2024). The grid resolutions of ME-IC/MIX, BVOC, UBVO, and PKU-NH<sub>3</sub> are 0.25°, 0.25°, 27 km, and 0.1°, respectively. The PM<sub>2.5</sub> profiles in Liu et al. (2017a) were used to convert PM<sub>2.5</sub> from non-shipping emissions to the AERO7 species. We multiplied the PM<sub>2.5</sub> emissions from the MEIC/MIX by the V and Ni fractions in PM<sub>2.5</sub> in China by source (Table S3) to obtain the V and Ni emissions from anthropogenic sources excluding shipping (Liu et al., 2018b). The source-specific vertical profiles for industrial, power, residential, and land-based transportation emissions in Table S6 were referenced from Zheng et al. (2019).

### 2.3 Observational data and evaluation of simulation results

The observational data from the national meteorological stations and the national air quality monitoring stations listed in Table S7 were used to evaluate the simulation results. The hourly meteorological data were downloaded from the website (<http://data.cma.cn>, last access: 9 December 2024), and the hourly air quality data were obtained from the China National Environmental Monitoring Centre (<https://air.cnemc.cn:18014>, last access: 9 December 2024). To evaluate the model performance for PM<sub>2.5</sub> in coastal areas, 21 port cities along the coast of China were selected as representatives. They rank among the top 20 in terms of cargo or container throughput nationwide and distribute on the coasts of the Bohai Rim (Dalian, Yingkou, Caofeidian, Binhai of Tianjin, and Yantai), the Yellow Sea (Qingdao, Rizhao, and Lianyungang), the Yangtze River Delta (Shanghai, Ningbo, Zhoushan, Hangzhou, Nantong, Zhangjiagang, and Nanjing), the Pearl River Delta (Shenzhen, Guangzhou, and Zhuhai), and the Beibu Gulf (Qinzhou), as well as on the west coast of the Taiwan Strait (Fuzhou and Xiamen). The simulated concentrations in the surface layer were used as a comparison with the observational data.

We used the hourly observational data from the Pudong site of Shanghai to evaluate the model performance of the tracers of ship emissions (V and Ni) and the secondary inorganic aerosols (SO<sub>4</sub><sup>2-</sup>, NO<sub>3</sub><sup>-</sup>, and NH<sub>4</sub><sup>+</sup>). The metallic elements and the ions were measured by the Model Xact 625 (Cooper Environmental Services, LLT, OR, USA) and the MARGA (Model ADI 2080, Applikon Analytical B. V. Corp., the Netherlands), respectively. Detailed information on the location of the monitoring site and the online instruments can be found elsewhere (Yu et al., 2021).

To quantify the model performances of the meteorological factors and the air pollutants, the Spearman's correla-

tion coefficient ( $r$ ), the normalized mean bias (NMB), the root-mean-square error (RMSE), and the index of agreement (IoA) were calculated.

### 3 Results and discussion

#### 3.1 Changes in ship emissions under the staged fuel oil policies

The emissions of SO<sub>2</sub>, NO<sub>x</sub>, CO, NMVOCs, PM<sub>2.5</sub>, V, and Ni from shipping in the CECA and inland waters of China from 2017 to 2021 were calculated based on the method introduced in Sect. 2.2.1 (Table 2). NO<sub>x</sub> is the major pollutant from shipping, and the nitrogen control policy was not changed nationwide in the study period. Hence, the amount of NO<sub>x</sub> emissions can be regarded as a proxy of ship traffic volume. As mentioned in Sect. 1, the variations in emissions in each April from 2017 to 2021 were used to represent the interannual variations. In the CECA and inland waters of China, the NO<sub>x</sub> emissions from shipping gradually increased from 2017 to 2020, with the largest increase (37.1 %) from 2017 to 2018, and then slightly decreased in 2021. Due to the increase in ship activities, the NO<sub>x</sub> emissions from shipping increased by 51.8 % from 2017 to 2021. Figure S1 depicts the spatial distributions of the SO<sub>2</sub> and NO<sub>x</sub> emissions from shipping in each April from 2017 to 2021, with high values along the major shipping routes of coastal China, the Yangtze River and its main branches, and the Pearl River. In April 2019, the higher emission intensity on the main route along the southeastern coast of China was due to the bypass behaviour that ships tend to navigate outside the CECA. For the seasonal patterns, in 2017, the NO<sub>x</sub> emissions from shipping were higher in April (114.1 kt) and October (112.1 kt) and smaller in July (101.6 kt) due to the fishing ban and reached the lowest value in January (89.9 kt) due to the Spring Festival. However, in 2021, the lowest value (128.9 kt) occurred in July, while January exhibited relatively high NO<sub>x</sub> emissions (169.2 kt), as the Spring Festival was in February.

By contrast, in the same area, the monthly average SO<sub>2</sub> (PM<sub>2.5</sub>) emissions from shipping decreased by 68.4 % (32.8 %) from 2017 to 2021 due to the IMO Regulation and China's inland sulfur regulation. The monthly average PM<sub>2.5</sub> emissions were reduced from 7.6 kt in 2017 to 5.1 kt in 2021. In addition, the monthly average V emissions from shipping experienced a dramatic drop (by 90.8 %) from 118.8 t in 2017 to 11.0 t in 2021. The monthly average Ni emissions decreased from 41.6 t in 2017 to 24.1 t in 2021, with a reduction of 42.0 %. The average V / Ni ratio decreased from 2.86 in 2017 to 0.46 in 2021. Figure S2 (Fig. S3) shows the interannual variations in V (Ni) emissions from shipping and anthropogenic sources excluding shipping. It can clearly be seen that higher V and Ni emissions transferred from nearshore waters to the outer border of the CECA in 2019.

Table S8 shows the contributions of ship emissions to the total anthropogenic emissions in China's 200 nm zone and

coastal provinces (coastal areas hereafter). The staged low sulfur policies since 2017 significantly reduced the SO<sub>2</sub>, V, and Ni emissions, and their reduction rates were larger than those from land-based anthropogenic sources, especially for V. The contributions of ship emissions to the total SO<sub>2</sub>, V, and Ni emissions in the coastal areas decreased from 13.9 %, 89.2 %, and 55.5 % in 2017 to 7.7 %, 56.0 %, and 53.8 % in 2021, respectively. The contribution of ship emissions to the total PM<sub>2.5</sub> emissions in the coastal areas remained at 4.0 %. However, the share of NO<sub>x</sub> emissions from shipping increased from 13.2 % in 2017 to 21.2 % in 2021 due to the increase in shipping activities and the reduction in emissions from land-based sources.

#### 3.2 Model performance

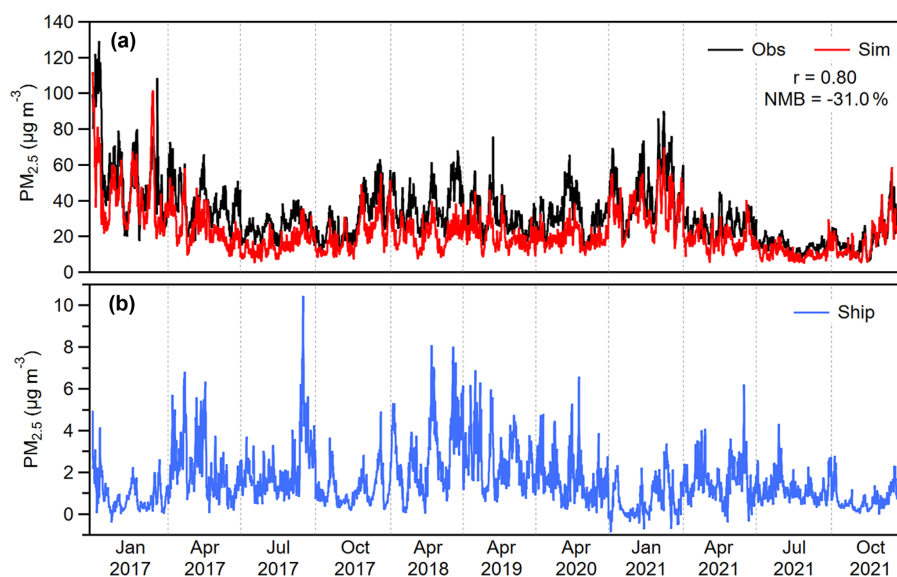
Uncertainties in simulation results of air quality can be caused by multiple factors, such as the accuracy of meteorological inputs, uncertainties in emission inventories, and the simplification of mechanisms in the model. The model performance of the meteorological elements was acceptable, with negative biases for relative humidity and positive biases for 10 m wind speed in most port cities (Table S9). The simulation results from the base runs were used to evaluate the model performance of the CMAQ model (Table S10). The biases of SO<sub>2</sub> and NO<sub>2</sub> were mainly caused by the uncertainties in local emissions of the MEIC inventory, which impacted on the simulation of secondary pollutants. The PM<sub>2.5</sub> concentrations were underestimated in all of the 21 port cities concerned, with an average NMB of −31.0 % (Fig. 2a), which was mainly attributed to the underestimation of secondary aerosols. Multiple causes, such as lack of chemical mechanisms, underestimation of atmospheric oxidants and NH<sub>3</sub> emissions, and overestimation of wind speed, may lead to the underestimation of secondary aerosols, especially nitrate (Table S11) (Sun et al., 2022; Xie et al., 2022). Nevertheless, the model can reproduce the temporal variation in mean PM<sub>2.5</sub> concentrations, with a correlation of  $r = 0.80$ . The model successfully reproduced the monthly average concentrations of V and Ni and the changing impacts of fuel oil policies on V and Ni in Shanghai (Table S12). The model could characterize the diurnal variation patterns of V, with higher values during the nighttime and lower values during the daytime (Fig. S4). The daily variations in simulation results were more pronounced than those based on observation, which was due to the overestimation of the diurnal cycle of the planetary boundary layer height (PBLH) using the YSU PBL scheme (Du et al., 2020). The updated V and Ni emissions were verified to be applicable on a national scale by comparing the observational data reported in several other coastal cities and the simulation results in this study (Table S13). More details on the model performance can be found in Text S3 in the Supplement.

For the shipping-related PM<sub>2.5</sub> concentrations in the concerned port cities, the mean value during the simulation pe-

**Table 2.** Time variation in emissions of SO<sub>2</sub>, NO<sub>x</sub>, CO, NMVOCs, PM<sub>2.5</sub>, V, and Ni from shipping in the coastal emission control area (CECA) and inland waters of China.

	SO <sub>2</sub> (kt)	NO <sub>x</sub> (kt)	CO (kt)	NMVOCs (kt)	PM <sub>2.5</sub> (kt)	V (t)	Ni (t)
January 2017	35.3	89.9	4.2	4.6	6.5	102.1	35.7
April 2017	44.4	114.1	5.4	6.0	8.3	130.7	45.7
July 2017	40.3	101.6	4.6	5.1	7.2	115.0	40.2
October 2017	43.5	112.1	5.3	5.9	8.2	127.4	44.7
April 2018	63.2	156.4	7.3	8.1	11.5	185.9	64.7
April 2019	13.2	166.7	8.1	8.9	5.3	51.1	29.1
April 2020	14.3	170.9	8.1	9.0	5.7	15.3	32.0
January 2021	13.8	169.2	8.2	8.6	5.4	12.1	26.4
April 2021	13.9	164.8	8.0	8.3	5.4	11.8	25.9
July 2021	10.4	128.9	6.1	6.2	4.0	8.2	18.3
October 2021	13.6	171.0	8.4	8.9	5.5	11.7	25.7
2017 average per month	40.9	104.4	4.9	5.4	7.6	118.8	41.6
2021 average per month	12.9	158.5	7.7	8.0	5.1	11.0	24.1

Note: average per month equals the average of emissions during January, April, July, and October.

**Figure 2.** Time series of hourly mean PM<sub>2.5</sub> concentrations during the simulation periods, averaged for the representative port cities of China: (a) observational data (Obs) and simulated results of base runs (Sim) and (b) simulated shipping-related PM<sub>2.5</sub>.

riods was  $1.6 \mu\text{g m}^{-3}$  (Fig. 2b). The hourly mean shipping-related PM<sub>2.5</sub> peaked on the early morning of 27 July 2017 (local time hereafter) with a concentration of  $10.4 \mu\text{g m}^{-3}$ , while the minimum value of  $-0.9 \mu\text{g m}^{-3}$  occurred on the morning of 2 January 2021. Using the zero-out method may obtain negative shipping-related PM<sub>2.5</sub> concentrations. Shipping is an emission sector releasing large amounts of NO<sub>x</sub> which can participate in complex non-linear chemistry. Ship-emitted NO<sub>x</sub> significantly consumes atmospheric oxidants, such as O<sub>3</sub> and various radicals (OH, HO<sub>2</sub>, RO<sub>2</sub>, etc.), in areas controlled by the VOC-limited regime. The potential reduction in these oxidants can inhibit the sec-

ondary aerosol formation, resulting in the negative simulated values of PM<sub>2.5</sub> related to ship emissions. It is noted that the shipping-related PM<sub>2.5</sub> concentration did not show significant reduction in 2019 compared to 2017 and 2018, which was likely due to the increase in the impact of secondary aerosols (Fig. 2b). This result is discussed further in Sect. 3.4.1.

### 3.3 Spatiotemporal patterns of the concentrations of gas precursors from shipping

SO<sub>2</sub> and NO<sub>2</sub> are the key gas precursors of secondary aerosols and the important pollutants from shipping; thus their spatiotemporal patterns are of interest. As SO<sub>2</sub> is a typical primary pollutant emitted by ships, it was selected to analyse the factors affecting the seasonal and interannual patterns such as emission intensity and meteorological conditions. Regarding the seasonal patterns, the highest SO<sub>2</sub> concentrations from shipping in most regions of China occurred in spring when the prevailing wind was weak and generally blew onshore in the areas with high ship emissions (Fig. S5). Meanwhile, the ship emissions in spring were at a high level:  $\sim 8\%$  higher than the annual average. We selected April as the representative month for the analysis of interannual variations nationwide; thus the policy shifts in advance in some port areas were not considered. In winter, the concentrations on the land showed higher values than those in spring due to the weak diffusion conditions. In the offshore areas, the concentrations in winter were not as high as those in spring, and this was caused by the significant winter monsoon. The concentrations in summer and autumn were relatively low, which was due to the dilution effect of the southeasterly monsoon in summer and the northeasterly cold air mass in autumn.

As April was selected as the representative month, the interannual variations in the SO<sub>2</sub> and NO<sub>2</sub> concentrations from shipping in each April from 2017 to 2021 are shown in Fig. 3. To study the general interannual variations during the policy stages, the 99th percentile ( $P_{99}$ ) values of the grids in the model domain were used in the following, and very high values on a local scale were not considered. The overall changes in the impact of ship emissions on the air pollutants by annual average from 2017 to 2021 can be found in the Supplement (Text S4).

The SO<sub>2</sub> concentrations from shipping experienced evident staged reduction. The  $P_{99}$  values from 2017 to 2021 were 4.1, 5.2, 2.6, 1.5, and  $1.2\ \mu\text{g m}^{-3}$  in chronological order. Comparing the concentrations in 2018 and 2019, it was found that the DECA 2.0 had the effect of halving the SO<sub>2</sub> concentrations from shipping. After 2020, hotspots with values over  $4\ \mu\text{g m}^{-3}$  were only found along the coast of Zhejiang with dense fishing activities. The  $P_{99}$  value in 2021 was even lower than that in 2020, which was related to the rebound of fishing activities after the COVID-19 lockdown in early 2020. Comparing the  $P_{99}$  values in 2019 and 2021, a reduction rate of 53.8 % was obtained due to the IMO Regulation and was comparable to that brought by the DECA 2.0. In Sect. 3.3 and 3.4, the effect evaluation for the DECA 2.0 was based on the difference between 2019 and 2018, while that for the IMO Regulation were based on the difference between 2021 and 2019. In the 5 years studied, the SO<sub>2</sub> concentrations from shipping over the Yellow Sea exhibited the lowest level in 2020, which was attributed to the decline of long-distance shipping between China and Korea and be-

tween southern and northern China caused by the COVID-19 lockdown.

The main source of the ambient NO<sub>2</sub> from shipping is the rapid oxidation of NO in ship plumes and the high concentrations still fixed on the main routes and ports. The  $P_{99}$  values in April from 2017 to 2021 were 14.1, 18.0, 18.8, 20.8, and  $18.3\ \mu\text{g m}^{-3}$  in chronological order. The impacts of the staged policy shifts on the  $P_{99}$  values were within  $\pm 5\%$ . The decrease in SO<sub>2</sub> and the increase in NO<sub>2</sub> are expected to affect the formation pathways of shipping-related secondary aerosols and the composition of shipping-related PM<sub>2.5</sub>.

### 3.4 Spatiotemporal patterns of shipping-related PM<sub>2.5</sub> and its components

#### 3.4.1 Fine particulate matter (PM<sub>2.5</sub>)

PM<sub>2.5</sub> related to ship emissions contains primary and secondary aerosols, and secondary aerosols lead to the difference in the spatiotemporal patterns between the gas precursors and PM<sub>2.5</sub>. Figure 4 shows the interannual variations in the shipping-related PM<sub>2.5</sub> concentrations in the spring of 2017–2021. The  $P_{99}$  value in the model domain in April 2017 was  $4.1\ \mu\text{g m}^{-3}$  and slightly increased to  $4.6\ \mu\text{g m}^{-3}$  in April 2018. The increase was relatively significant over the Pearl River Estuary and the coastal waters of Zhejiang due to the increase in shipping activities.

Owing to the DECA 2.0 policy, in April 2019, the  $P_{99}$  value was reduced to  $3.7\ \mu\text{g m}^{-3}$ , with a reduction rate of 19.5 % year on year. This reduction rate was significantly lower than that of the primary PM<sub>2.5</sub> emissions from shipping (53.8 %). There was even an increase along the coast of Shandong province. It was found that high values were closer to the coastline during the DECA 2.0 period compared to during the DECA 1.0 period. This pattern was similar to the shipping-related NO<sub>3</sub><sup>−</sup> and NH<sub>4</sub><sup>+</sup> which can be seen in Sect. 3.4.3. In NH<sub>3</sub>-rich port areas, the increasing NO<sub>x</sub> emissions from shipping resulted in more nitrate formation. Meanwhile, the reduction in the SO<sub>2</sub> emissions provided more opportunities for HNO<sub>3</sub> to react with NH<sub>3</sub>. In addition, the difference between the shipping-related PM<sub>2.5</sub> concentrations inside and outside the CECA border was much smaller compared to the SO<sub>2</sub> concentrations from shipping, which was due to the onshore transport of aged aerosols from marine areas outside the CECA where high sulfur fuel oils were still used. These aged aerosols could also contribute to the shipping-related PM<sub>2.5</sub> in the port cities. Therefore, the impact of secondary aerosols partly offset the effect of primary PM emission reduction during the DECA 2.0 period.

In April 2020, due to the IMO Regulation, the  $P_{99}$  value decreased to  $3.3\ \mu\text{g m}^{-3}$ . The concentrations declined in most marine areas, especially the Yellow Sea, in which the main routes were not included in the CECA before 2020. In April 2021, ship emissions were more evenly distributed as the pandemic impact was limited. The concentrations of



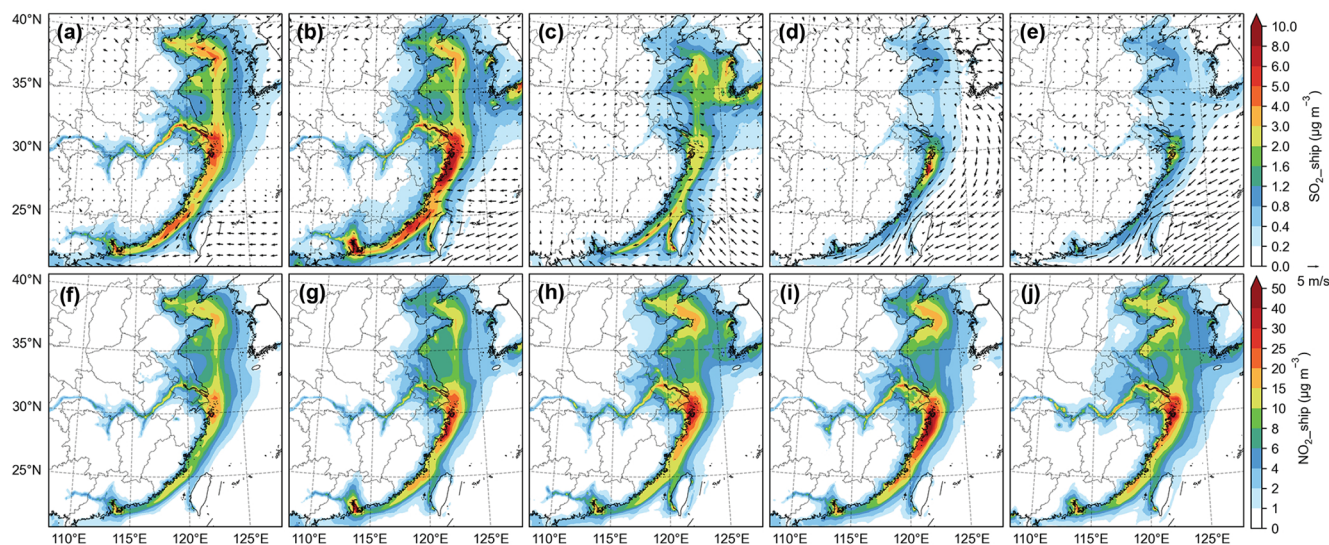


**Figure 3.** Impacts of ship emissions on (a–e) the SO<sub>2</sub> concentrations (SO<sub>2</sub>\_ship) and the simulated monthly average wind fields and (f–j) the NO<sub>2</sub> concentrations (NO<sub>2</sub>\_ship) in April from 2017 to 2021 in chronological order from left to right.

shipping-related PM<sub>2.5</sub> only presented relatively high values at a city level, with a  $P_{99}$  value of  $2.4 \mu\text{g m}^{-3}$  in coastal Zhejiang. Comparing the  $P_{99}$  values in 2021 and 2019, a reduction rate of 35.6 % was achieved due to the policy shift from the DECA 2.0 to the IMO Regulation.

The result in Lv et al. (2018) showed that the increased PM<sub>2.5</sub> concentration in China caused by shipping was up to  $5.2 \mu\text{g m}^{-3}$  in 2015. The values in this study were  $3.8 \mu\text{g m}^{-3}$  in 2017 and  $2.6 \mu\text{g m}^{-3}$  in 2021, demonstrating the decreasing trend in the shipping-related PM<sub>2.5</sub> concentrations under the staged fuel oil policies in China (Fig. S6).

Figure 5 shows the interannual variations in the contributions of ship emissions to ambient PM<sub>2.5</sub> concentrations. The  $P_{99}$  values in April from 2017 to 2021 were 26.7 %, 29.3 %, 34.3 %, 22.2 %, and 17.2 % in chronological order. It is of interest that the contributions near the coast of China in 2019 were even higher than those in 2018, although the concentrations were lower in 2019. These high values in 2019 were related to the increase in the shipping-related PM<sub>2.5</sub> concentrations outside the CECA border and to the decrease in the PM<sub>2.5</sub> concentrations related to land-based sources. Lower values in remote marine areas were related to the contribution of sea salt (Fig. S7).

The seasonal patterns of the absolute and relative impacts of ship emissions on PM<sub>2.5</sub> are shown in Figs. 6 and S8, respectively. The shipping-related PM<sub>2.5</sub> concentrations exhibited higher values in summer and spring and lower values in autumn and winter, which was different from those of the SO<sub>2</sub> and NO<sub>2</sub> concentrations from shipping. The key factor was the conversion rates of gas precursors to secondary aerosols. In summer, despite the better diffusion conditions, hotspots were found in coastal marine areas, which was likely due to secondary organic aerosol (SOA) formation

(see Sect. 3.4.4). In winter, it is worth noting that the values in most of northern China did not exceed  $0.5 \mu\text{g m}^{-3}$  and were even lower than  $0.1 \mu\text{g m}^{-3}$  in some coastal areas, which was very different from the pattern of SO<sub>2</sub> from shipping. NH<sub>3</sub> is consumed by SO<sub>2</sub> and NO<sub>x</sub> from land-based emissions prior to ship emissions; thus the formation of secondary aerosols related to shipping is inhibited, and this is called the domination effect by land-based sources. Regarding the relative impact of shipping-related PM<sub>2.5</sub>, the seasonal pattern generally showed a decreasing trend in summer, spring, autumn, and winter in the model domain, which was mainly due to the impact of the East Asian monsoon on the relative spatial distribution of ship- and land-based emissions.

### 3.4.2 Trace elements (V and Ni)

V and Ni are strongly correlated with SO<sub>2</sub> among the chemical species emitted by ships; thus their concentrations from shipping share similar spatiotemporal patterns (Fig. 7). In the model domain, the  $P_{99}$  values of the PM<sub>2.5</sub>-bound V (Ni) concentrations from shipping in April from 2017 to 2021 were 18.1 (5.6), 23.8 (7.4), 13.3 (5.0), 2.7 (5.0), and 2.1 (3.9)  $\text{ng m}^{-3}$  in chronological order. The reduction rate of the V (Ni) concentrations from shipping caused by the policy shift from the DECA 1.0 to 2.0 was 44.1 % (33.3 %), while a further reduction rate of 84.5 % (21.6 %) was achieved due to the IMO Regulation. The relative changes in the V and Ni concentrations from shipping were different. The V / Ni ratios in ambient particles from shipping decreased from  $\sim 3.0$  to  $\sim 0.5$  from 2017 to 2021. Despite the sharp reduction in the concentrations of V and Ni from shipping, shipping is still an important source of the ambient V and Ni under the current fuel oil regulations. The contributions of ship emis-

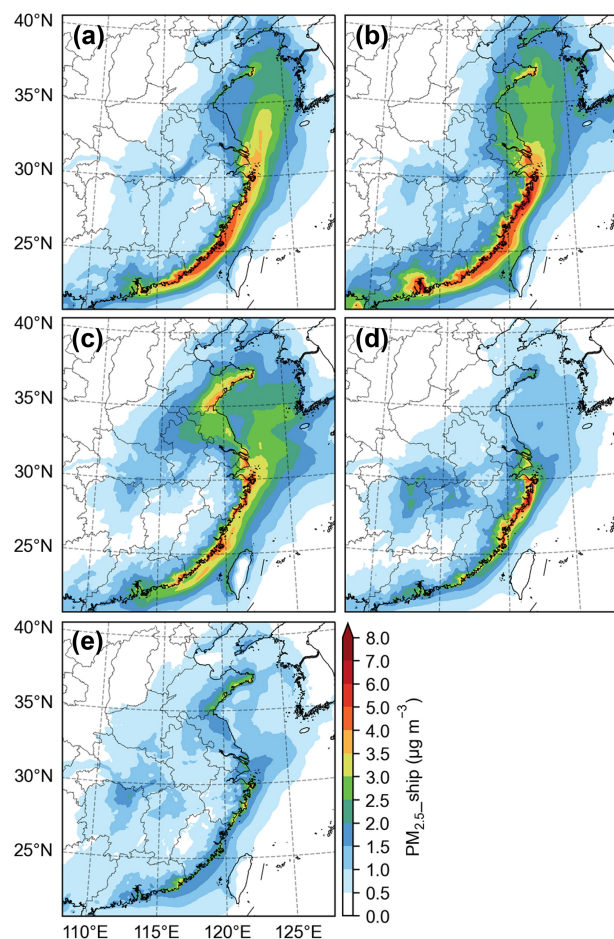


**Figure 4.** Interannual variations in the potential impacts of ship emissions on PM<sub>2.5</sub> (PM<sub>2.5</sub>\_ship) concentrations in April of (a) 2017, (b) 2018, (c) 2019, (d) 2020, and (e) 2021.

sions to the concentrations of V and Ni could exceed 50 % along the coast in 2021 (Figs. S9 and S10).

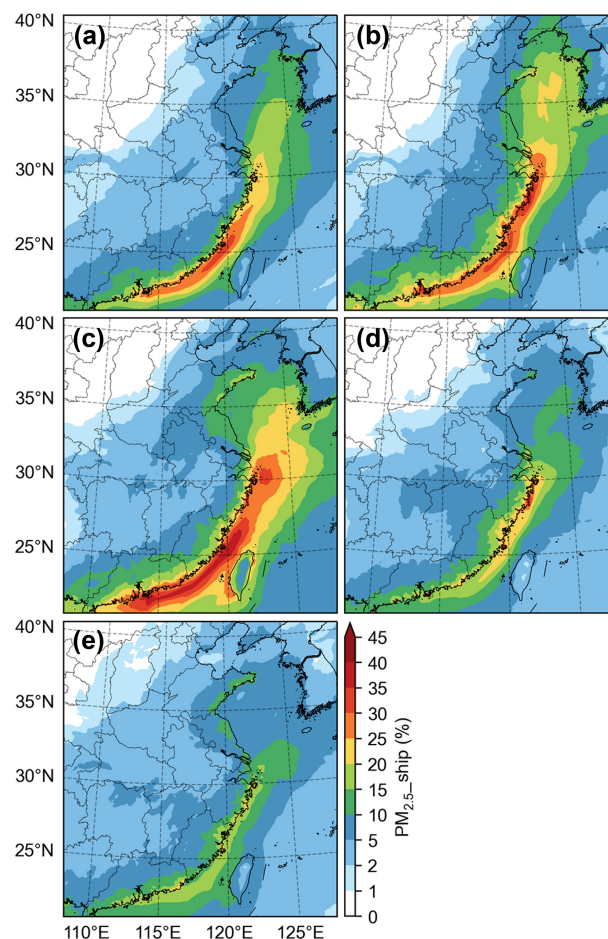


**Figure 5.** Interannual variations in the contributions of ship emissions to PM<sub>2.5</sub> concentrations (PM<sub>2.5</sub>\_ship%) in April of (a) 2017, (b) 2018, (c) 2019, (d) 2020, and (e) 2021.

### 3.4.3 Secondary inorganic aerosols

Sulfate ( $\text{SO}_4^{2-}$ ), nitrate ( $\text{NO}_3^-$ ), and ammonium ( $\text{NH}_4^+$ ), known as SNA for short, are the most important secondary inorganic species in PM<sub>2.5</sub>. Their concentrations are highly related to the concentrations and the conversion rates of gas precursors, including  $\text{SO}_2$ ,  $\text{NO}_x$ , and  $\text{NH}_3$ . Their spatiotemporal variations are shown in Fig. 8. Given that PM<sub>2.5</sub>, especially secondary species such as nitrate, was underestimated in China's coastal cities in this study as discussed in Sect. 3.2, the simulated concentrations of SNA related to ship emissions were conservative.

For the formation of sulfate, the main atmospheric oxidant is hydroxyl radical (OH), which transforms  $\text{SO}_2$  to  $\text{H}_2\text{SO}_4$ . Then,  $\text{H}_2\text{SO}_4$  is neutralized by  $\text{NH}_3$  forming  $(\text{NH}_4)_2\text{SO}_4$  or dissolves in aerosol liquid water and binds with positive ions such as  $\text{Na}^+$ . As EC is a stable species, the primary sulfate concentration from shipping can be calculated through multiplying the EC concentration from shipping by the ratio of  $\text{SO}_4^{2-}$  to EC in ship-emitted PM in Table S4. Thus, the sec-



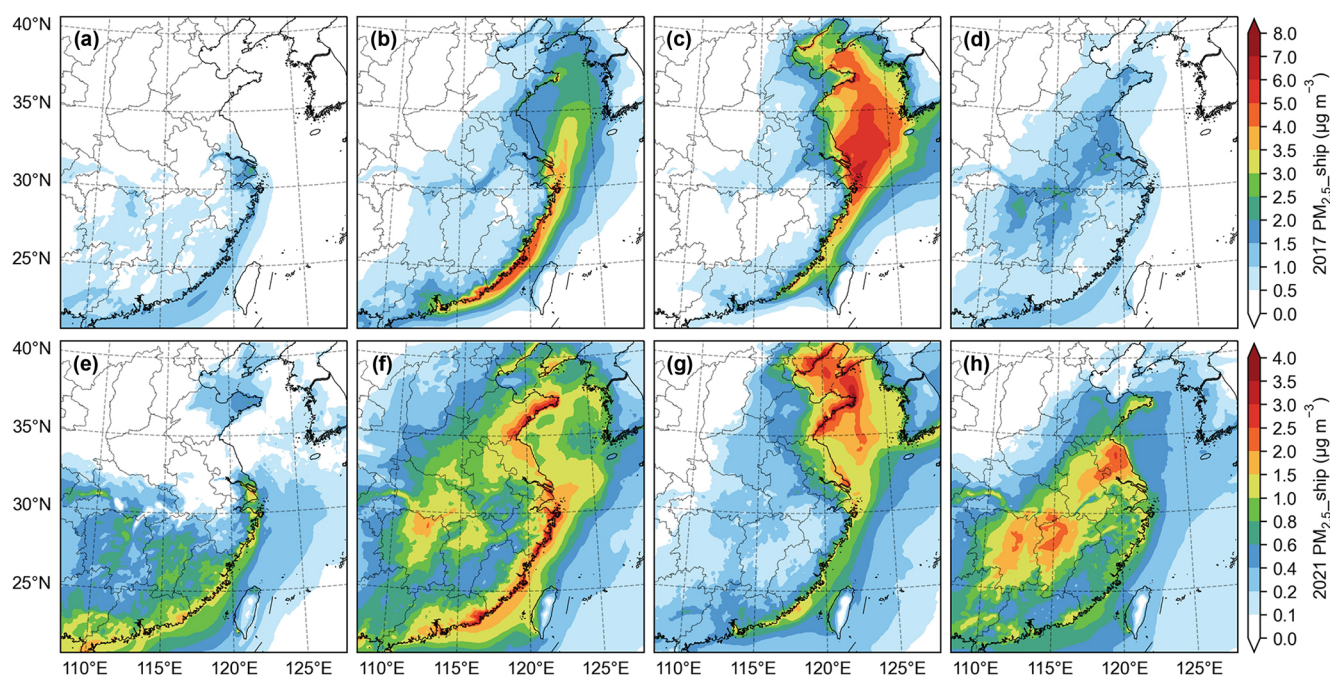


**Figure 6.** Seasonal patterns of the potential impacts of ship emissions on PM<sub>2.5</sub> (PM<sub>2.5</sub>\_ship) concentrations in (a) January, (b) April, (c) July, and (d) October of 2017 and (e) January, (f) April, (g) July, and (h) October of 2021.

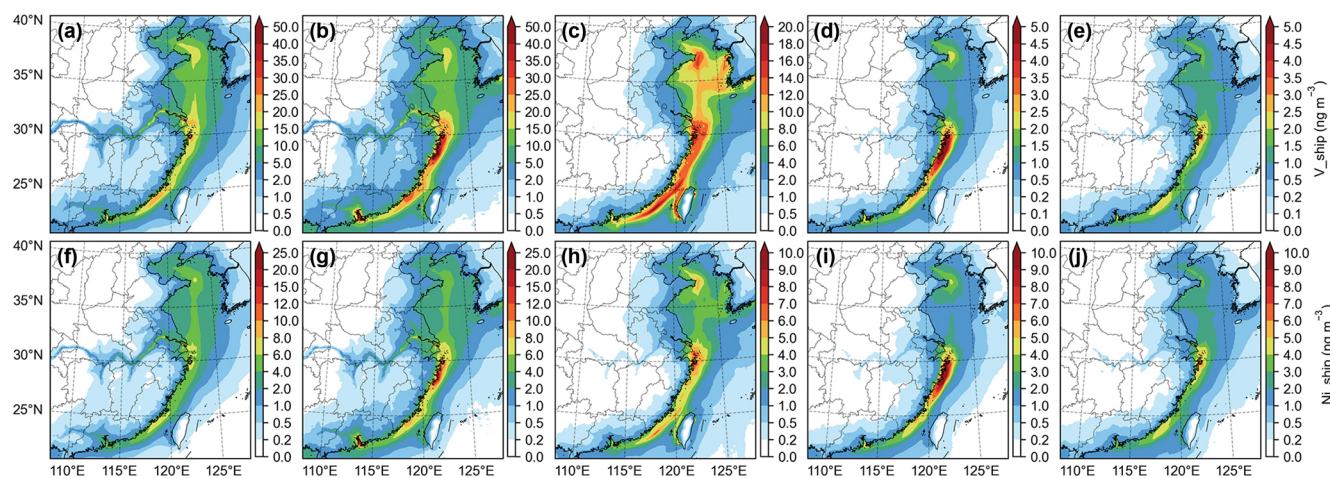


**Figure 7.** Impacts of ship emissions on (a–e) the V concentrations (V<sub>ship</sub>) and (f–i) the Ni concentrations (Ni<sub>ship</sub>) in April from 2017 to 2021 in chronological order from left to right.

ondary part of shipping-related sulfate equals the difference of the total concentration and the primary part. Based on this assumption, it was found that primary sulfate emitted by ships played a minor role, while secondary sulfate accounted for 80 %–90 % of the shipping-related sulfate regardless of the policy shift.

The  $P_{99}$  values of the shipping-related sulfate concentrations from 2017 to 2021 were 1.5, 1.8, 1.5, 0.5, and  $0.5 \mu\text{g m}^{-3}$  in chronological order. Due to the policy shift from the DECA 1.0 to 2.0, the  $P_{99}$  value of the sulfate con-

centrations only decreased by 15.8 %, and the decrease rate was significantly lower compared to the SO<sub>2</sub> concentrations (49.7 %). During the DECA 2.0 period, the SO<sub>2</sub> emissions outside the CECA were still at a high level and had the potential to generate sulfate in the onshore transport processes, which partly offset the impact of SO<sub>2</sub> emission reduction in the CECA. The  $P_{99}$  value of the sulfate concentrations was then reduced by 66.1 % due to the policy shift from the DECA 2.0 to the IMO Regulation. After 2020, the SO<sub>2</sub> emis-



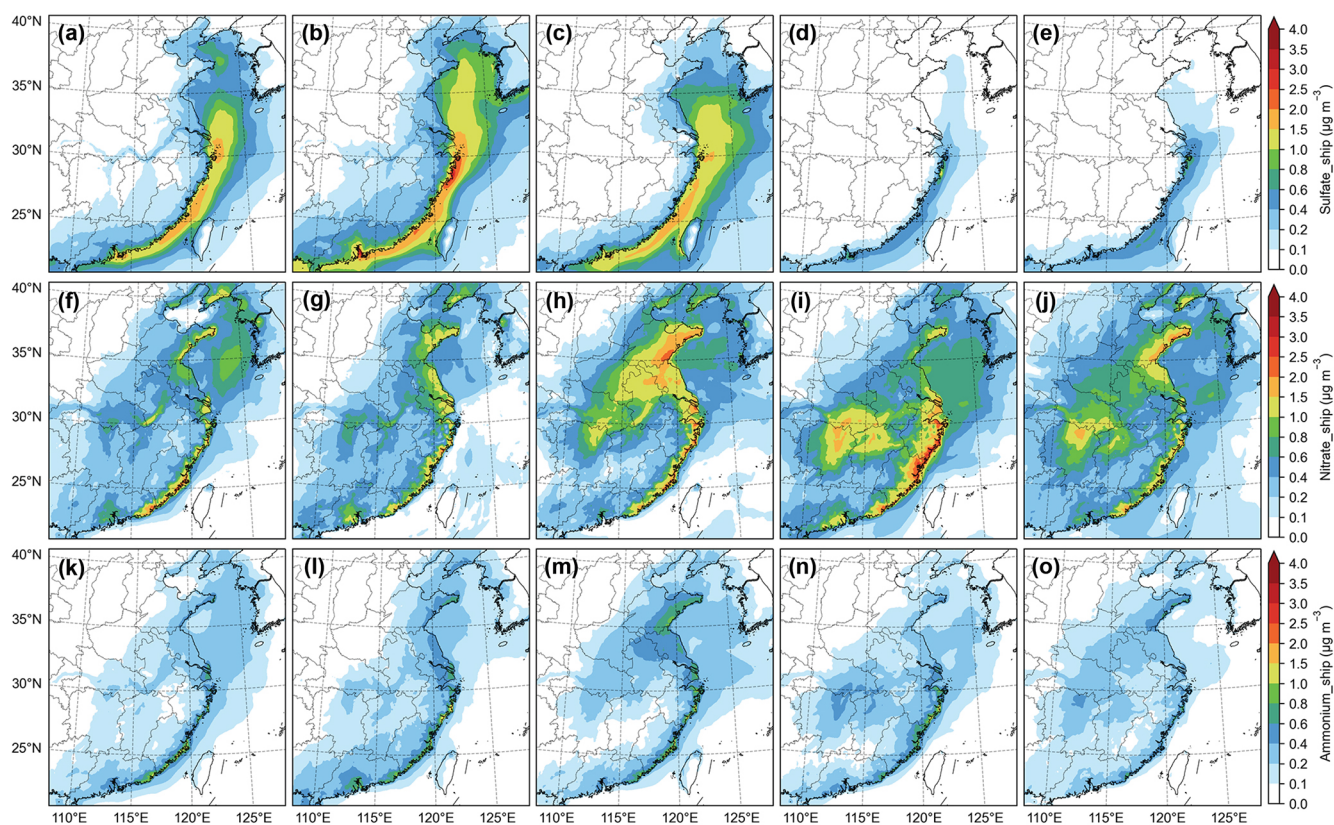


**Figure 8.** Potential impacts of ship emissions on (a–e) the sulfate concentrations (Sulfate\_ship), (f–j) the nitrate concentrations (Nitrate\_ship), and (k–o) the ammonium concentrations (Ammonium\_ship) in April from 2017 to 2021 in chronological order from left to right.

sions outside the CECA sharply decreased, and the offset effect no longer existed.

Most of initially emitted NO<sub>x</sub> is in the form of NO, and is rapidly oxidized to NO<sub>2</sub>. During the daytime, NO<sub>2</sub> can be converted to HNO<sub>3</sub> by reacting with OH radicals. During the nighttime, NO<sub>2</sub> combines with NO<sub>3</sub> radicals originating from the oxidation of NO<sub>2</sub> by O<sub>3</sub> to generate dinitrogen pentoxide (N<sub>2</sub>O<sub>5</sub>). HNO<sub>3</sub> is formed via the reaction of N<sub>2</sub>O<sub>5</sub> and water. Compared to HNO<sub>3</sub>, NH<sub>3</sub> preferentially reacts with H<sub>2</sub>SO<sub>4</sub> because (NH<sub>4</sub>)<sub>2</sub>SO<sub>4</sub> is more stable than NH<sub>4</sub>NO<sub>3</sub>. Therefore, the formation of particulate nitrate requires sufficient amounts of NH<sub>3</sub>. The difference in the formation mechanisms between sulfate and nitrate can explain the significant difference in the spatial patterns of the concentrations between SO<sub>4</sub><sup>2−</sup> and NO<sub>3</sub><sup>−</sup> related to ship emissions. High SO<sub>4</sub><sup>2−</sup> concentrations were found in coastal marine areas with plenty of radicals, whereas high NO<sub>3</sub><sup>−</sup> concentrations generally occurred along the coast with sufficient NH<sub>3</sub> emissions. The *P*<sub>99</sub> values of the shipping-related NO<sub>3</sub><sup>−</sup> concentrations showed a similar interannual variation pattern compared to the NO<sub>2</sub> concentrations, with values of 1.2, 1.1, 1.7, 1.8, and 1.4 µg m<sup>−3</sup> from 2017 to 2021 year by year. During the DECA 2.0 period, the decrease in SO<sub>2</sub> emissions

provided more opportunities for HNO<sub>3</sub> to be neutralized by NH<sub>3</sub>, leading to the noticeable increase in the concentrations of shipping-related NO<sub>3</sub><sup>−</sup> over the land areas of eastern China. In the same way, in the inland emission control areas, the concentrations of shipping-related NO<sub>3</sub><sup>−</sup> shipping over the middle reaches of the Yangtze River in 2020 and 2021 under the ultra-low sulfur regulation were remarkably higher than those in 2017 and 2018. In this study, there was no markedly negative value of shipping-related NO<sub>3</sub><sup>−</sup> in the model domain, which differed from the result in the Mediterranean Sea also based on the CMAQ model (Fink et al., 2023a). This was caused by the huge amounts of NH<sub>3</sub> emissions from agriculture in China, providing ammonia-rich conditions to generate NH<sub>4</sub>NO<sub>3</sub> (Fig. S11).

The spatial patterns of shipping-related NH<sub>4</sub><sup>+</sup> were similar to those of shipping-related NO<sub>3</sub><sup>−</sup> because NH<sub>3</sub> is essential to the formation of particulate nitrate. This result also implied that the relatively high levels of shipping-related SO<sub>4</sub><sup>2−</sup> in ammonia-poor offshore areas tended to present in the form of metal salt such as Na<sub>2</sub>SO<sub>4</sub> rather than (NH<sub>4</sub>)<sub>2</sub>SO<sub>4</sub>. Compared to SO<sub>4</sub><sup>2−</sup> and NO<sub>3</sub><sup>−</sup>, the concentration of shipping-related NH<sub>4</sub><sup>+</sup> was at a lower level due to the much smaller molar mass. The *P*<sub>99</sub> values varied little from year to year, with



the values of 0.6, 0.7, 0.7, 0.6, and 0.5  $\mu\text{g m}^{-3}$  from 2017 to 2021, which was due to the balance between the decrease in the sulfate concentrations and the increase in the nitrate concentrations.

### 3.4.4 Organic aerosols

Organic aerosol (OA) is categorized into primary organic aerosol (POA) and secondary organic aerosol (SOA). POA is calculated as the sum of particulate organic carbon (POC) and particulate non-carbon organic matter (PNCOM), two species in the AERO7 module. The spatial pattern of the POA concentrations from shipping was similar to that of the SO<sub>2</sub> concentrations from shipping (Fig. 9a–e). The  $P_{99}$  values in the spring of 2017–2021 were 0.3, 0.4, 0.3, 0.1, and 0.1  $\mu\text{g m}^{-3}$  in chronological order. The  $P_{99}$  value was reduced by 34.7 % and further by 57.4 % due to the staged policy shifts. In this study, the sum of the contributions of POC and PNCOM to primary PM<sub>2.5</sub> emitted by ships using HSFO was set to 70.8 %, while this value was reduced to 33.4 % in the case of burning LSFO (Table S4). Thus, the reduction in the POA concentrations from shipping due to the fuel type change was more significant compared to the total shipping-related PM<sub>2.5</sub> concentrations.

SOA, a kind of photochemical product, is produced via the reactions of VOCs or semi-volatile organic compounds (SVOCs) with atmospheric oxidants. The  $P_{99}$  values of the shipping-related SOA concentrations from 2017 to 2021 were 1.6, 1.9, 1.3, 0.5, and 0.5  $\mu\text{g m}^{-3}$  year by year and were 4–5 times as much as those of the POA concentrations from shipping (Fig. 9f–j). The  $P_{99}$  value was reduced by 29.6 % and further by 60.8 % due to the staged policy shifts, which was comparable to the pattern of the POA concentrations from shipping.

The summertime hotspots of the shipping-related PM<sub>2.5</sub> concentrations corresponded to the high SOA concentrations in the eastern offshore areas (Fig. S12). In summer, high temperatures and good lighting conditions are in favour of BVOC emissions and photochemical reactions, resulting in abundant oxidants in the background atmosphere to generate O<sub>3</sub>, sulfate, and SOA. Ship emissions could increase the concentrations of O<sub>3</sub> and SOA in the NO<sub>x</sub>-limited marine atmosphere with low NO<sub>x</sub> concentrations. Although the NO<sub>x</sub> and VOC emissions from shipping increased from 2017 to 2021, the shipping-related SOA concentrations in summer decreased. This result suggested that the decrease in the shipping-related PM was likely to reduce the impact of gas-particle partitioning of organic matter with low to medium volatility. The potential impact of ship emissions on SOA showed negative values in inland areas in the winter of 2021, which was indirectly caused by the O<sub>3</sub> titration by NO<sub>x</sub> under the VOC-limited regime.

## 3.5 Intercomparison of the impacts over the port cities

In Sect. 3.5, the perspective is shifted from a regional scale to an urban scale. For each of the 21 port cities selected in this study, the data of the grids where populous downtown areas (instead of the ports themselves) are located were extracted for the analysis on the impacts of ship emissions. Thus, the results can reflect the role of ship emissions in the presence of large amounts of land-based emissions in urban areas.

### 3.5.1 Effects of the IMO Regulation

Figure 10 shows the absolute and relative impacts of ship emissions on multiple species, such as SO<sub>2</sub>, NO<sub>2</sub>, PM<sub>2.5</sub>, SO<sub>4</sub><sup>2-</sup>, NO<sub>3</sub><sup>-</sup>, NH<sub>4</sub><sup>+</sup>, carbonaceous aerosol (CA, referred to as the sum of OA and EC), V, and Ni, at the annual average level in China's main port cities in 2017 and 2021. On average, across all the cities concerned with 95 % confidence intervals (CIs), the SO<sub>2</sub> concentration from shipping was reduced from  $1.3 \pm 0.4 \mu\text{g m}^{-3}$  in 2017 to  $0.48 \pm 0.12 \mu\text{g m}^{-3}$  in 2021 due to the IMO Regulation. Its reduction rate was 63.3 %, close to the reduction rate of SO<sub>2</sub> emissions from shipping in the CECA and inland areas of China (68.4 %). The share of the SO<sub>2</sub> concentration from shipping was  $(14.3 \pm 5.5) \%$  in 2017 and decreased to  $(9.0 \pm 4.0) \%$  in 2021. However, the NO<sub>2</sub> concentration from shipping increased from  $4.3 \pm 1.1$  to  $7.1 \pm 5.6 \mu\text{g m}^{-3}$  due to the growth in shipping activities. The increase rate (65.9 %) was higher than that of the NO<sub>x</sub> emissions from shipping (51.8 %), because ship emissions increased the atmospheric oxidation capacity in offshore areas and more NO could be oxidized to NO<sub>2</sub>. The share of the NO<sub>2</sub> concentration from shipping rose from  $(13.9 \pm 5.6) \%$  to  $(22.6 \pm 6.2) \%$ .

The shipping-related PM<sub>2.5</sub> concentration was reduced from  $1.6 \pm 0.2$  to  $1.1 \pm 0.1 \mu\text{g m}^{-3}$ , and the reduction rate (32.7 %) was very close to that of the PM<sub>2.5</sub> emissions from shipping (32.8 %). The shipping-related PM<sub>2.5</sub> concentrations at the city level ranged from 0.8  $\mu\text{g m}^{-3}$  in QZ to 2.7  $\mu\text{g m}^{-3}$  in ZS in 2017 and from 0.6  $\mu\text{g m}^{-3}$  in YK to 1.6  $\mu\text{g m}^{-3}$  in QD in 2021. It is noted that only QZ experienced an increase, though very small, which corresponded to the intense growth in cargo throughput of the Beibu Gulf ports approaching 100 % in the past 6 years. After the operation of the Pinglu Canal at the end of 2026, there is still great potential for the increase in the impacts of ship emissions on air quality in this area. Compared to SO<sub>2</sub> and NO<sub>2</sub>, the contribution of ship emissions to the total PM<sub>2.5</sub> concentration only showed a slight change from  $(6.8 \pm 1.6) \%$  to  $(5.5 \pm 1.0) \%$ . The shipping-related PM<sub>2.5</sub> shares at the city level ranged from 3.0 % in YK to 17.4 % in ZS in 2017 and from 2.5 % in NJ to 10.3 % in ZS in 2021. Unexpectedly, they showed slight increases in five cities adjacent to the Yellow Sea, including DL, YT, QD, RZ, and LYG, which was in accordance with the increase in the shipping-related NO<sub>3</sub><sup>-</sup> and NH<sub>4</sub><sup>+</sup> concentration shares.

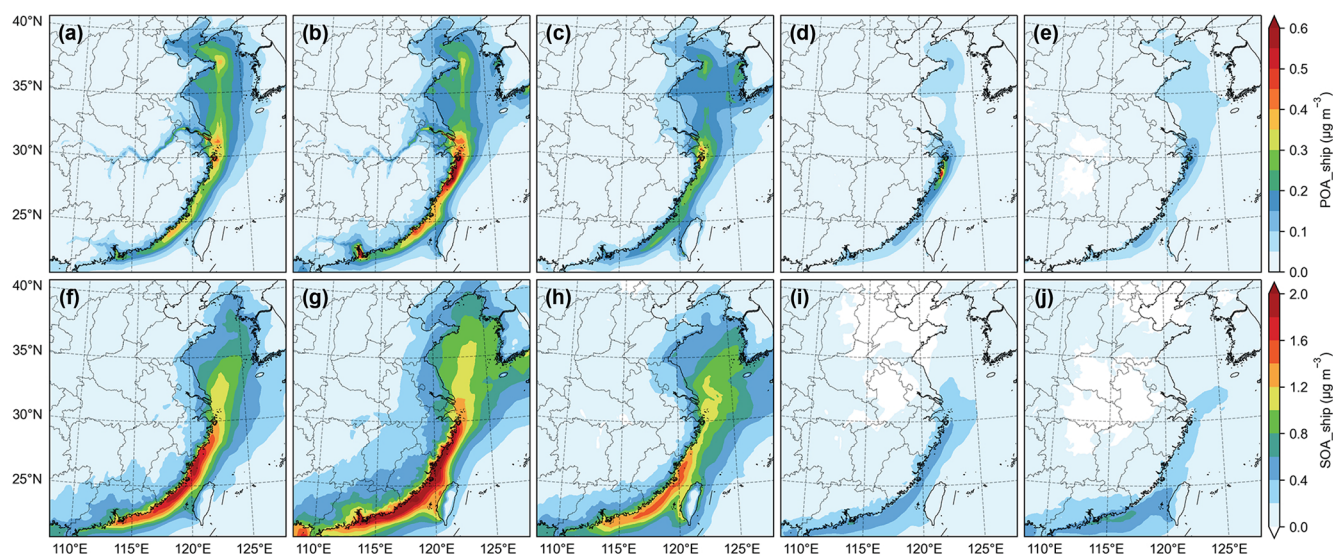


**Figure 9.** Potential impacts of ship emissions on the concentrations of (a–e) primary organic aerosols (POA<sub>ship</sub>) and (f–j) secondary organic aerosols (SOA<sub>ship</sub>) in April from 2017 to 2021 in chronological order from left to right.

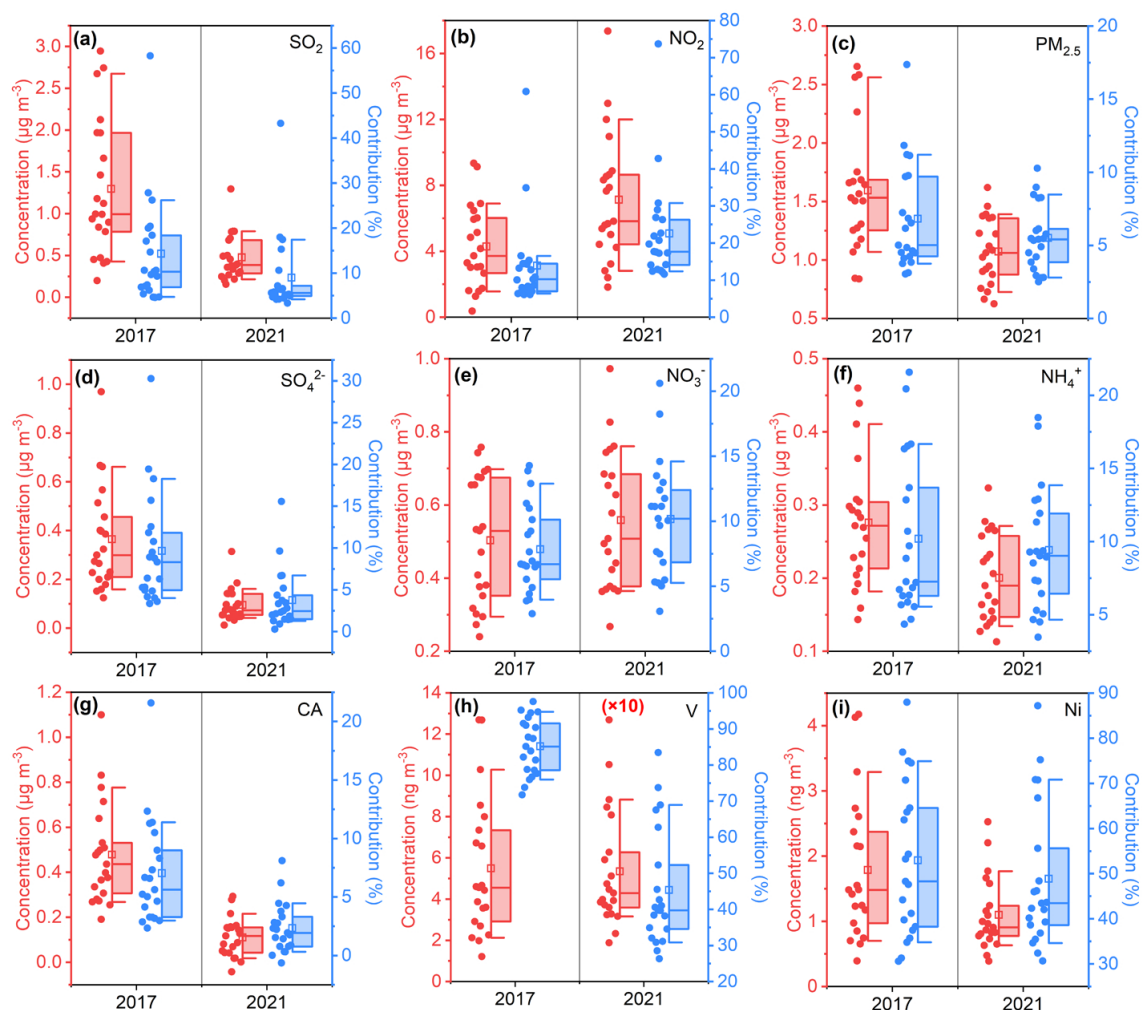
For the chemical species in the shipping-related PM<sub>2.5</sub>, the SO<sub>4</sub><sup>2−</sup> concentration was reduced from  $0.4 \pm 0.1$  to  $0.1 \pm 0.0 \mu\text{g m}^{-3}$ , with the reduction rate of 74.0 %, higher than that of the SO<sub>2</sub> concentration from shipping. In contrast, the shipping-related NO<sub>3</sub><sup>−</sup> concentration increased by 11.0 % from  $0.5 \pm 0.0$  to  $0.6 \pm 0.1 \mu\text{g m}^{-3}$ . Nevertheless, its increase rate was much smaller than that of the NO<sub>2</sub> concentration from shipping, indicating a low nitrogen oxidation rate (NOR). The weakened sulfate formation was demonstrated by the decrease in the contribution of the secondary SO<sub>4</sub><sup>2−</sup> to the total SO<sub>4</sub><sup>2−</sup> related to shipping from  $(90.0 \pm 2.0) \%$  to  $(77.7 \pm 10.0) \%$ . Because the decrease in SO<sub>4</sub><sup>2−</sup> was more significant than the increase in NO<sub>3</sub><sup>−</sup>, the shipping-related NH<sub>4</sub><sup>+</sup> concentration decreased by 28.6 % from  $0.3 \pm 0.0$  to  $0.2 \pm 0.0 \mu\text{g m}^{-3}$ . The shipping-related CA concentration decreased from  $0.5 \pm 0.1$  to  $0.1 \pm 0.0 \mu\text{g m}^{-3}$ , with a reduction rate of 76.9 %, even higher than that of SO<sub>4</sub><sup>2−</sup>. The V concentration from shipping sharply dropped from  $5.5 \pm 1.5$  to  $0.5 \pm 0.1 \text{ ng m}^{-3}$ . In comparison, the Ni concentration from shipping decreased moderately from  $1.8 \pm 0.5$  to  $1.1 \pm 0.2 \text{ ng m}^{-3}$ . The reduction rates of the V and Ni concentrations from shipping were 90.3 % and 38.4 %, respectively, close to the reduction rates of the emissions of V (90.8 %) and Ni (42.0 %) from shipping. In addition, the relative impacts of ship emissions on the concentrations of SO<sub>4</sub><sup>2−</sup>, NO<sub>3</sub><sup>−</sup>, NH<sub>4</sub><sup>+</sup>, CA, V, and Ni were  $(9.6 \pm 3.0) \%$ ,  $(7.9 \pm 1.5) \%$ ,  $(10.2 \pm 2.4) \%$ ,  $(7.0 \pm 2.0) \%$ ,  $(85.2 \pm 3.5) \%$ , and  $(52.9 \pm 7.6) \%$  in 2017 and  $(3.8 \pm 1.6) \%$ ,  $(10.2 \pm 2.0) \%$ ,  $(9.4 \pm 1.8) \%$ ,  $(2.4 \pm 0.9) \%$ ,  $(45.4 \pm 7.3) \%$ , and  $(48.9 \pm 7.1) \%$  in 2021, respectively. Among the six species, only NO<sub>3</sub><sup>−</sup> exhibited an increasing trend in the relative impact.

Figure 11 presents the simulated chemical speciation of PM<sub>2.5</sub> from all sectors and shipping over China's main port cities in 2017 and 2021. Six categories of chemical species contributing more than 95 % to PM<sub>2.5</sub> were considered, including SO<sub>4</sub><sup>2−</sup>, NO<sub>3</sub><sup>−</sup>, NH<sub>4</sub><sup>+</sup>, POA, SOA, and soil. Soil, a variable in the CMAQ model output, is calculated following Eq. (1):

$$\begin{aligned} \text{soil} = & 2.20 \times \text{Al} + 3.48 \times \text{Si} + 1.63 \times \text{Ca} + 2.42 \times \text{Fe} \\ & + 1.94 \times \text{Ti}. \end{aligned} \quad (1)$$

The change in the characteristics of the shipping-related PM<sub>2.5</sub> components was far more significant compared to the PM<sub>2.5</sub> derived by the base runs. SO<sub>4</sub><sup>2−</sup> accounted for  $(21.2 \pm 2.8) \%$  in the shipping-related PM<sub>2.5</sub> averaged for the port cities concerned in 2017 and decreased to  $(9.3 \pm 2.4) \%$  in 2021, while the percentage of SO<sub>4</sub><sup>2−</sup> in the PM<sub>2.5</sub> from all sectors only decreased from  $(16.7 \pm 1.3) \%$  to  $(15.0 \pm 0.9) \%$ . This result is regarded as the potential impact and does not suggest that ship-emitted PM<sub>2.5</sub> contains less sulfate content than PM<sub>2.5</sub> from land-based sources. The SO<sub>4</sub><sup>2−</sup> shares displayed lower values in the northern region and higher values in the southern region, which may be partly related to the lower aerosol acidity in the northern region (Wang et al., 2022).

In the low-sulfur era, ship emissions tend to enhance the nitrate formation in the high-HNO<sub>3</sub> and high-NH<sub>3</sub> but low-H<sub>2</sub>SO<sub>4</sub> conditions in China's coastal cities. Accordingly, NO<sub>3</sub><sup>−</sup> has become the major component of the shipping-related PM<sub>2.5</sub>, with the average NO<sub>3</sub><sup>−</sup> share increasing from  $(32.2 \pm 4.8) \%$  to  $(54.7 \pm 5.0) \%$ . The NH<sub>4</sub><sup>+</sup> share also showed an increasing trend from  $(17.0 \pm 0.8) \%$  to  $(19.6 \pm 1.3) \%$  as the decrease in the SO<sub>4</sub><sup>2−</sup> share cannot offset the increase in the NO<sub>3</sub><sup>−</sup> share. In comparison, in



**Figure 10.** Impacts of ship emissions on (a) SO<sub>2</sub>, (b) NO<sub>2</sub>, (c) PM<sub>2.5</sub>, (d) SO<sub>4</sub><sup>2-</sup>, (e) NO<sub>3</sub><sup>-</sup>, (f) NH<sub>4</sub><sup>+</sup>, (g) carbonaceous aerosol (CA), (h) V, and (i) Ni over the representative port cities of China in 2017 and 2021. The concentration boxes are coloured in red corresponding to the left axes, while the contribution boxes are coloured in blue corresponding to the right axes. Box plots show the mean (square), the median (–), the lower and upper quartiles (boxes), and the 10th and 90th percentiles (whiskers) of the simulated results. The V concentrations in 2021 are multiplied by 10.

the PM<sub>2.5</sub> from all sectors, the NO<sub>3</sub><sup>-</sup> share slightly increased from  $(28.1 \pm 2.6) \%$  to  $(30.5 \pm 2.5) \%$ , while the NH<sub>4</sub><sup>+</sup> share changed little from  $(12.2 \pm 0.6) \%$  to  $(11.8 \pm 0.8) \%$ . The sum of SNA share in the shipping-related PM<sub>2.5</sub> rose from  $(70.4 \pm 2.8) \%$  to  $(83.6 \pm 4.2) \%$ , whereas that in the PM<sub>2.5</sub> from all sectors remained at the same level of  $\sim 57 \%$ . The PM<sub>2.5</sub> pollution from shipping, which coastal urban areas suffer, is mainly caused by the transport and ageing processes of pollutants emitted by ships in the atmosphere from water to land, which can explain the higher SNA share in the shipping-related PM<sub>2.5</sub>.

For the organic aerosols, their contribution to shipping-related PM<sub>2.5</sub> decreased from  $(28.5 \pm 2.7) \%$  to  $(10.6 \pm 3.7) \%$ . The SOA share decreased from  $(21.8 \pm 2.6) \%$  to  $(5.3 \pm 3.6) \%$ , and the decrease in the

SOA share was much more significant than that in the POA share. The EC share increased from  $(0.7 \pm 0.2) \%$  to  $(1.8 \pm 0.4) \%$ , corresponding to the increase in the mapping factors of particulate EC (PEC) for ship emissions from 4.1 % to 7.0 %. Due to the substantial contribution of SNA, the EC shares in the shipping-related PM<sub>2.5</sub> were significantly lower than those in the primary PM<sub>2.5</sub> from shipping.

### 3.5.2 Roles of the meteorological factors

Meteorological factors can affect both physical and chemical processes of atmospheric pollutants. Considering the complexity of non-linear chemistry discussed above, we focused on the physical aspects here to clarify the roles of meteorological factors in the spatiotemporal patterns of primary PM



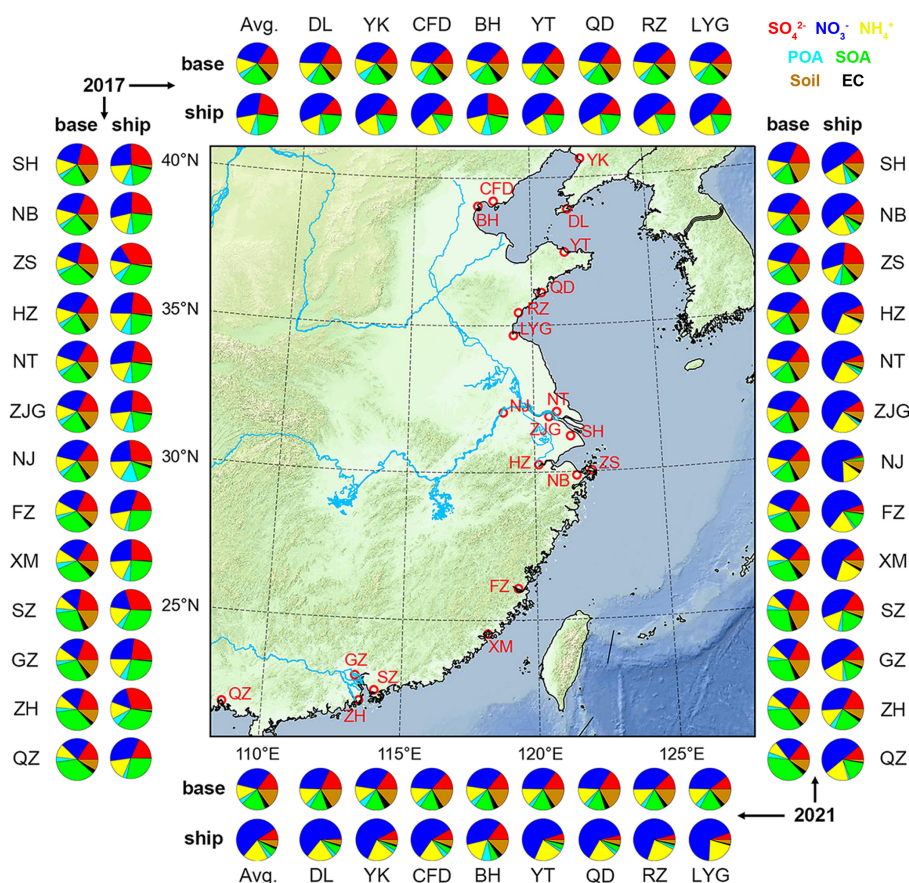


**Figure 11.** Simulated chemical speciation of PM<sub>2.5</sub> from all sectors (base) and shipping (ship) over the representative main port cities of China in 2017 (left and top) and 2021 (right and bottom). Avg. denotes the annual average. DL, YK, CFD, BH, YT, QD, RZ, LYG, SH, NB, ZS, HZ, NT, ZJG, NJ, FZ, XM, SZ, GZ, ZH, and QZ are the abbreviations of Dalian, Yingkou, Caofeidian, Binhai, Yantai, Qingdao, Rizhao, Lianyungang, Shanghai, Ningbo, Zhoushan, Hangzhou, Nantong, Zhangjiagang, Nanjing, Fuzhou, Xiamen, Shenzhen, Guangzhou, Zhuhai, and Qinzhou, respectively. The cities in the northern region are placed at the top and bottom, while the cities in the southern region are placed on the left and right.

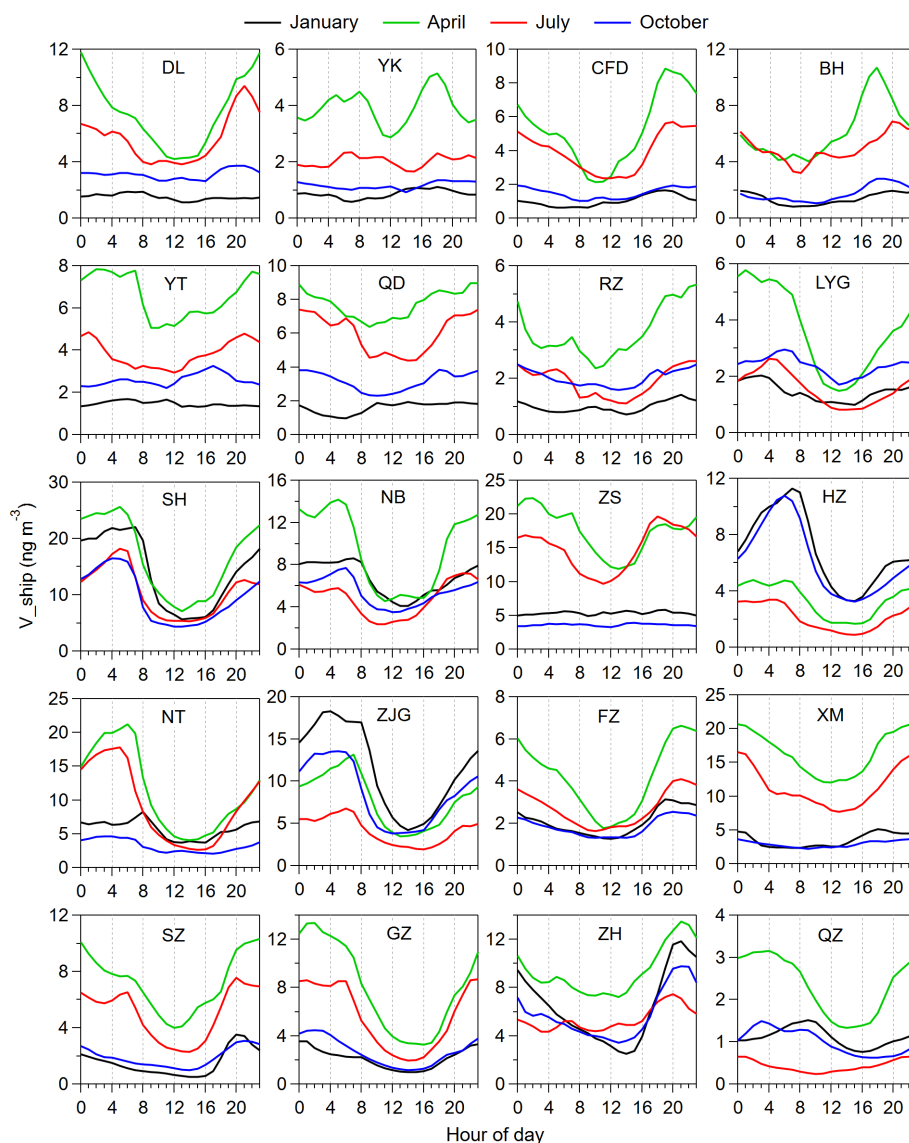
from shipping in the port cities concerned. We utilized V as the tracer, since V is the most convincing tracer of ship emissions and does not participate in any chemical process in the model. The impact of temporal variations in emissions was removed because the monthly ship emissions were evenly allocated by hour in this study. Although this simplification smoothed out the time series of the impacts of ship emissions, it contributed to the discussion on the effects of meteorological factors such as wind patterns and the PBLH. Ship emission inventories will be produced in hourly resolution based on the AIS data and used in monthly to long-term simulations in our future work.

Figure 12 delineates the diurnal variations in the V concentration from shipping over the port cities in every season of 2017 when ship emissions dominated the sources of ambient V. The lowest values occurred at noon in most cases, corresponding to the highest PBLH. However, the time when the highest values appeared showed significant differences by city, even by season in the same city. If the PBLH plays

a crucial role, the V concentration will simply increase with the reduction in the PBLH and reach the peak level in the early morning. This pattern was found in four cities in the YRD, including SH, HZ, NT, and ZJG, in every season. A secondary peak during 20:00–21:00 UTC+8. was observed in SH in summer, though subtle, which was caused by the intrusion of the sea breeze after the dissipation of the daytime weak convergence (Shang et al., 2019; Zhai et al., 2023). SH is more likely to be affected by large synoptic systems, and urbanization results in a weaker land breeze pattern; meanwhile, the contribution of inland ship emissions is considerable in downtown SH. The simulation results confirmed the findings in our previous study conducted in SH based on field observations (Yu et al., 2021).

In ZH, SZ, and FZ, the V concentrations from shipping peaked before midnight with values significantly higher than those during the early morning in every season, indicating that the sea–land breeze circulation (SLBC) significantly affected the diurnal patterns in these cities, especially ZH. The





**Figure 12.** Simulated diurnal variations in the V concentrations from shipping ( $V_{\text{ship}}$ ) over the representative port cities of China in January, April, July, and October of 2017.

SLBC impact in downtown GZ was much weaker than that in ZH and SZ, which was due to the dense inland shipping activities in GZ. In BH, CFD, and YK, three ports located in Bohai Bay, the SLBC impact was significant in at least three seasons. In comparison, the SLBC impact was smaller in QD and RZ, two cities adjacent to the Yellow Sea. Nevertheless, this impact was found in every season: the land breeze could block the transport of ship emissions from marine areas and counteract the PBL compression effect. In DL and YT, the SLBC impact was noticeable in summer and autumn. The SLBC impact was found in a certain season, such as summer in NB and ZS or winter in XM. This study adopted the grid resolution of 9 km and still characterized the SLBC, a type of local-scale system. The results in this study

are rather different from those in a study conducted in the eastern United States with scarce SLBC impacts using the WRF-CAMx (Golbazi and Archer, 2023).

In addition, the seasonal variations in the V concentrations from shipping in the port cities are also shown in Fig. 12. The concentration peaked in spring in most of the cities due to the weak onshore airflows. SH, ZS, NT, FZ, and XM, located along the eastern to southeastern coast, exhibited the lowest levels in autumn. The lowest levels were observed in winter for all the northern cities affected by the prevailing northwesterly wind and for two southern cities (GZ and SZ) affected by the prevailing northeasterly wind. The winter monsoon was adverse to the transport of ship emissions to these cities. In the other cities, poor diffusion conditions enhanced

the wintertime concentration levels. It is of interest that cities close in distance did not always show the same seasonal pattern. For example, in the YRD, NB and ZS, adjacent to each other, showed different seasonal patterns. The southerly wind in July was conducive to the transport of pollutants emitted by ships in NB to ZS, whereas the northerly wind in January and the northeasterly wind in October had an opposite effect. In addition to the airflow intensity, the relationship between areas with high ship emissions and prevailing airflow directions is an important factor affecting the seasonal pattern of the concentrations of primary PM emitted by ships in receptor cities. Combined with the result that secondary aerosols dominate the PM<sub>2.5</sub> concentrations from shipping, our findings suggest that it is important to consider both transport pathways and secondary aerosol formation mechanisms to combat the PM<sub>2.5</sub> pollution caused by shipping in different regions.

#### 4 Conclusions

To meet the requirements of the IMO Regulation, China carried out staged fuel oil policies for seagoing vessels, including the DECA 1.0 and the DECA 2.0, which came into effect in 2017 and 2019, respectively. In addition, the inland emission control areas were implemented in 2019 and became more stringent in 2020. It is of significance to evaluate the effects of the staged policies on air quality in China. We updated the ship emission inventory in China to 2021 based on the AIS data. The emissions of V and Ni from shipping were constrained by the field observational data and the results of on-board emission measurements. The WRF/CMAQ model was utilized to simulate the impacts on PM<sub>2.5</sub> in China and its gas precursors (SO<sub>2</sub> and NO<sub>2</sub>) and components from 2017 to 2021 based on the zero-out method.

In the CECA and inland areas of China, the SO<sub>2</sub>, PM<sub>2.5</sub>, V, and Ni emissions from shipping were reduced by 68.4 %, 32.8 %, 90.8 %, and 42.0 %, respectively, from 2017 to 2021 due to the IMO Regulation and China's inland river emission control areas. However, the NO<sub>x</sub> emissions from shipping increased by 51.8 % due to the increase in shipping activities.

At the domain level, due to the policy shift from the DECA 1.0 to the DECA 2.0, the *P*<sub>99</sub> values of the concentrations of SO<sub>2</sub>, PM<sub>2.5</sub>, V, Ni, SO<sub>4</sub><sup>2-</sup>, POA, and SOA contributed by shipping were reduced by 49.7 %, 19.5 %, 44.1 %, 33.3 %, 15.8 %, 34.7 %, and 29.6 %, respectively. The reduction rate of PM<sub>2.5</sub> was significantly lower than that of SO<sub>2</sub>, which was attributed to the increase in NH<sub>4</sub>NO<sub>3</sub> along the coast and the transport of aged aerosols with high sulfur content from the marine areas outside the CECA. Due to the policy shift from the DECA 2.0 to the IMO Regulation, they further decreased by 53.8 %, 35.6 %, 84.5 %, 21.6 %, 66.1 %, 57.4 %, and 60.8 %, respectively. However, the impacts of the staged policy shifts on the *P*<sub>99</sub> values of the NO<sub>2</sub> concentrations from shipping were within ±5 %. Regarding the annual av-

erage, ship emissions increased the PM<sub>2.5</sub> concentrations up to 3.8 µg m<sup>-3</sup> in 2017 and 2.6 µg m<sup>-3</sup> in 2021 along China's coastal areas. The seasonal pattern of the shipping-related PM<sub>2.5</sub> concentrations was mainly affected by the seasonality of secondary aerosol formation, whereas that of the contributions of ship emissions to the PM<sub>2.5</sub> concentrations was driven by the East Asian monsoon.

At the city level, the contributions of ship emissions to the PM<sub>2.5</sub> concentration over China's main port cities ranged from 3.0 % to 17.4 % in 2017 and 2.5 % to 10.3 % in 2021. The change rates of the concentrations of PM<sub>2.5</sub>, SO<sub>4</sub><sup>2-</sup>, NO<sub>3</sub><sup>-</sup>, NH<sub>4</sub><sup>+</sup>, carbonaceous aerosols, V, and Ni related to ship emissions were -32.7 %, -74.0 %, +11.0 %, -27.5 %, -76.9 %, -90.3 %, and -38.4 %, respectively. NO<sub>3</sub><sup>-</sup> has become the dominant species, accounting for 54.6 % of the shipping-related PM<sub>2.5</sub> after 2020. The increasing NO<sub>x</sub> emissions from shipping and their potential impacts on PM<sub>2.5</sub> and O<sub>3</sub> are of concern, which calls for the expansion of the Tier III Regulation in more coastal waters worldwide. In addition, the sea-land breeze circulation played an important role in the diurnal patterns of the concentrations of primary particulate matter from shipping in most seaports. Our findings suggest that it is important to consider both transport pathways and secondary aerosol formation mechanisms to combat the PM<sub>2.5</sub> pollution caused by shipping in different regions.

**Data availability.** The data derived from the ship emission model and the WRF/CMAQ model presented in this paper can be obtained from Yan Zhang (yan\_zhang@fudan.edu.cn) upon request.

**Supplement.** The supplement related to this article is available online at <https://doi.org/10.5194/acp-25-9497-2025-supplement>.

**Author contributions.** GY: investigation, methodology, software, validation, formal analysis, data curation, visualization, funding acquisition, and writing (original draft preparation). YZ: conceptualization, investigation, supervision, methodology, validation, project administration, funding acquisition, and writing (review and editing). QW: validation, data curation, and writing (review). ZH: methodology, software, and data curation. SJ: methodology, software, and data curation. FY: data curation, funding acquisition, and writing (review). XY: writing (review and editing). CH: supervision, data curation, and writing (review and editing).

**Competing interests.** The contact author has declared that none of the authors has any competing interests.

**Disclaimer.** Publisher's note: Copernicus Publications remains neutral with regard to jurisdictional claims made in the text, published maps, institutional affiliations, or any other geographical rep-

resentation in this paper. While Copernicus Publications makes every effort to include appropriate place names, the final responsibility lies with the authors. Regarding the maps used in this paper, please note that Figs. 1, 3–9, and 11 contain disputed territories.

**Acknowledgements.** The work was supported by the National Natural Science Foundation of China (grant no. 42077195); the Natural Science Foundation of Shanghai Committee of Science and Technology, China (grant no. 22ZR1407700); and the Science and Technology Innovation Action Plan of Shanghai (grant no. 24YF2736200).

**Financial support.** The work was funded by the National Natural Science Foundation of China (grant no. 42077195); the Natural Science Foundation of Shanghai Committee of Science and Technology, China (grant no. 22ZR1407700); and the Science and Technology Innovation Action Plan of Shanghai (grant no. 24YF2736200).

**Review statement.** This paper was edited by Toshihiko Take-mura and reviewed by two anonymous referees.

## References

- Agrawal, H., Welch, W. A., Miller, J. W., and Cocker, D. R.: Emission Measurements from a Crude Oil Tanker at Sea, *Environ. Sci. Technol.*, 42, 7098–7103, <https://doi.org/10.1021/es703102y>, 2008a.
- Agrawal, H., Malloy, Q. G. J., Welch, W. A., Wayne Miller, J., and Cocker, D. R.: In-use gaseous and particulate matter emissions from a modern ocean going container vessel, *Atmos. Environ.*, 42, 5504–5510, 2008b.
- Agrawal, H., Eden, R., Zhang, X., Fine, P. M., Katzenstein, A., Miller, J. W., Ospital, J., Teffera, S., and Cocker, D. R.: Primary Particulate Matter from Ocean-Going Engines in the Southern California Air Basin, *Environ. Sci. Technol.*, 43, 5398–5402, <https://doi.org/10.1021/es8035016>, 2009.
- Agrawal, H., Welch, W. A., Henningsen, S., Miller, J. W., and Cocker, D. R.: Emissions from main propulsion engine on container ship at sea, *J. Geophys. Res.*, 115, D23205, <https://doi.org/10.1029/2009jd013346>, 2010.
- Aksoyoglu, S., Baltensperger, U., and Prévôt, A. S. H.: Contribution of ship emissions to the concentration and deposition of air pollutants in Europe, *Atmos. Chem. Phys.*, 16, 1895–1906, <https://doi.org/10.5194/acp-16-1895-2016>, 2016.
- Anastasopoulos, A. T., Sofowote, U. M., Hopke, P. K., Rouleau, M., Shin, T., Dheri, A., Peng, H., Kulka, R., Gibson, M. D., Farah, P. M., and Sundar, N.: Air quality in Canadian port cities after regulation of low-sulphur marine fuel in the North American Emissions Control Area, *Sci. Total Environ.*, 791, 147949, <https://doi.org/10.1016/j.scitotenv.2021.147949>, 2021.
- Badeke, R., Matthias, V., Karl, M., and Grawe, D.: Effects of vertical ship exhaust plume distributions on urban pollutant concentration – a sensitivity study with MITRAS v2.0 and EPISODE-CityChem v1.4, *Geosci. Model Dev.*, 15, 4077–4103, <https://doi.org/10.5194/gmd-15-4077-2022>, 2022.
- Celo, V., Dabek-Zlotorzynska, E., and McCurdy, M.: Chemical characterization of exhaust emissions from selected Canadian marine vessels: the case of trace metals and lanthanoids, *Environ. Sci. Technol.*, 49, 5220–5226, <https://doi.org/10.1021/acs.est.5b00127>, 2015.
- Chosson, F., Paoli, R., and Cuenot, B.: Ship plume dispersion rates in convective boundary layers for chemistry models, *Atmos. Chem. Phys.*, 8, 4841–4853, <https://doi.org/10.5194/acp-8-4841-2008>, 2008.
- Corbin, J. C., Mensah, A. A., Pieber, S. M., Orasche, J., Michalke, B., Zanatta, M., Czech, H., Massabo, D., Buatier de Mongeot, F., Mennucci, C., El Haddad, I., Kumar, N. K., Stengel, B., Huang, Y., Zimmermann, R., Prevot, A. S. H., and Gysel, M.: Trace Metals in Soot and PM<sub>2.5</sub> from Heavy-Fuel-Oil Combustion in a Marine Engine, *Environ. Sci. Technol.*, 52, 6714–6722, <https://doi.org/10.1021/acs.est.8b01764>, 2018.
- Dalsøren, S. B., Eide, M. S., Endresen, Ø., Mjelde, A., Gravir, G., and Isaksen, I. S. A.: Update on emissions and environmental impacts from the international fleet of ships: the contribution from major ship types and ports, *Atmos. Chem. Phys.*, 9, 2171–2194, <https://doi.org/10.5194/acp-9-2171-2009>, 2009.
- Du, Q., Zhao, C., Zhang, M., Dong, X., Chen, Y., Liu, Z., Hu, Z., Zhang, Q., Li, Y., Yuan, R., and Miao, S.: Modeling diurnal variation of surface PM<sub>2.5</sub> concentrations over East China with WRF-Chem: impacts from boundary-layer mixing and anthropogenic emission, *Atmos. Chem. Phys.*, 20, 2839–2863, <https://doi.org/10.5194/acp-20-2839-2020>, 2020.
- EMSA and EEA: European Maritime Transport Environmental Report 2021, European Maritime Safety Agency (EMSA) and European Environment Agency (EEA), <https://doi.org/10.2800/3525>, 2021.
- Eyring, V., Isaksen, I. S. A., Berntsen, T., Collins, W. J., Corbett, J. J., Endresen, O., Grainger, R. G., Moldanova, J., Schlager, H., and Stevenson, D. S.: Transport impacts on atmosphere and climate: Shipping, *Atmos. Environ.*, 44, 4735–4771, <https://doi.org/10.1016/j.atmosenv.2009.04.059>, 2010.
- Fan, Q., Zhang, Y., Ma, W., Ma, H., Feng, J., Yu, Q., Yang, X., Ng, S. K., Fu, Q., and Chen, L.: Spatial and Seasonal Dynamics of Ship Emissions over the Yangtze River Delta and East China Sea and Their Potential Environmental Influence, *Environ. Sci. Technol.*, 50, 1322–1329, <https://doi.org/10.1021/acs.est.5b03965>, 2016.
- Feng, J., Zhang, Y., Li, S., Mao, J., Patton, A. P., Zhou, Y., Ma, W., Liu, C., Kan, H., Huang, C., An, J., Li, L., Shen, Y., Fu, Q., Wang, X., Liu, J., Wang, S., Ding, D., Cheng, J., Ge, W., Zhu, H., and Walker, K.: The influence of spatiality on shipping emissions, air quality and potential human exposure in the Yangtze River Delta/Shanghai, China, *Atmos. Chem. Phys.*, 19, 6167–6183, <https://doi.org/10.5194/acp-19-6167-2019>, 2019.
- Feng, X., Ma, Y., Lin, H., Fu, T. M., Zhang, Y., Wang, X., Zhang, A., Yuan, Y., Han, Z., Mao, J., Wang, D., Zhu, L., Wu, Y., Li, Y., and Yang, X.: Impacts of Ship Emissions on Air Quality in Southern China: Opportunistic Insights from the Abrupt Emission Changes in Early 2020, *Environ. Sci. Technol.*, 57, 16999–17010, <https://doi.org/10.1021/acs.est.3c04155>, 2023.
- Fink, L., Karl, M., Matthias, V., Oppo, S., Kranenburg, R., Kuenen, J., Jutterström, S., Moldanova, J., Majamäki, E., and Jalkanen, J.-P.: A multimodel evaluation of the potential impact of shipping on particle species in the Mediterranean Sea, *Atmos. Chem.*

- Phys., 23, 10163–10189, <https://doi.org/10.5194/acp-23-10163-2023>, 2023a.
- Fink, L., Karl, M., Matthias, V., Oppo, S., Kranenburg, R., Kuenen, J., Moldanova, J., Jutterström, S., Jalkanen, J.-P., and Majamäki, E.: Potential impact of shipping on air pollution in the Mediterranean region – a multimodel evaluation: comparison of photooxidants NO<sub>2</sub> and O<sub>3</sub>, *Atmos. Chem. Phys.*, 23, 1825–1862, <https://doi.org/10.5194/acp-23-1825-2023>, 2023b.
- Fu, X., Chen, D., Wang, X., Li, Y., Lang, J., Zhou, Y., and Guo, X.: The impacts of ship emissions on ozone in eastern China, *Sci. Total Environ.*, 903, 166252, <https://doi.org/10.1016/j.scitotenv.2023.166252>, 2023.
- Golbazi, M. and Archer, C.: Impacts of maritime shipping on air pollution along the US East Coast, *Atmos. Chem. Phys.*, 23, 15057–15075, <https://doi.org/10.5194/acp-23-15057-2023>, 2023.
- He, L., Wang, J., Liu, Y., Zhang, Y., He, C., Yu, Q., and Ma, W.: Selection of onshore sites based on monitoring possibility evaluation of exhausts from individual ships for Yantian Port, China, *Atmos. Environ.*, 247, 118187, <https://doi.org/10.1016/j.atmosenv.2021.118187>, 2021.
- Hersbach, H., Bell, B., Berrisford, P., Biavati, G., Horányi, A., Muñoz Sabater, J., Nicolas, J., Peubey, C., Radu, R., Rozum, I., Schepers, D., Simmons, A., Soci, C., Dee, D., and Thépaut, J.-N.: ERA5 hourly data on single levels from 1940 to present, Copernicus Climate Change Service (C3S) Climate Data Store (CDS) [data set], <https://doi.org/10.24381/cds.adbb2d47>, 2023.
- Huang, C., Hu, Q., Wang, H., Qiao, L., Jing, S., Wang, H., Zhou, M., Zhu, S., Ma, Y., Lou, S., Li, L., Tao, S., Li, Y., and Lou, D.: Emission factors of particulate and gaseous compounds from a large cargo vessel operated under real-world conditions, *Environ. Pollut.*, 242, 667–674, <https://doi.org/10.1016/j.envpol.2018.07.036>, 2018a.
- Huang, C., Hu, Q., Li, Y., Tian, J., Ma, Y., Zhao, Y., Feng, J., An, J., Qiao, L., Wang, H., Jing, S., Huang, D., Lou, S., Zhou, M., Zhu, S., Tao, S., and Li, L.: Intermediate Volatility Organic Compound Emissions from a Large Cargo Vessel Operated under Real-World Conditions, *Environ. Sci. Technol.*, 52, 12934–12942, <https://doi.org/10.1021/acs.est.8b04418>, 2018b.
- IMO: Fourth IMO GHG Study 2020, International Maritime Organization (IMO), London, UK, [https://greenvoyage2050.imo.org/wp-content/uploads/2021/07/Fourth-IMO-GHG-Study-2020-Full-report-and-annexes\\_compressed.pdf](https://greenvoyage2050.imo.org/wp-content/uploads/2021/07/Fourth-IMO-GHG-Study-2020-Full-report-and-annexes_compressed.pdf) (last access: 13 May 2025), 2021.
- Jang, E., Choi, S., Yoo, E., Hyun, S., and An, J.: Impact of shipping emissions regulation on urban aerosol composition changes revealed by receptor and numerical modelling, *npj Clim. Atmos. Sci.*, 6, 52, <https://doi.org/10.1038/s41612-023-00364-9>, 2023.
- Jiang, S., Zhang, Y., Yu, G., Han, Z., Zhao, J., Zhang, T., and Zheng, M.: Source-resolved atmospheric metal emissions, concentrations, and deposition fluxes into the East Asian seas, *Atmos. Chem. Phys.*, 24, 8363–8381, <https://doi.org/10.5194/acp-24-8363-2024>, 2024.
- Jonson, J. E., Gauss, M., Schulz, M., Jalkanen, J.-P., and Fagerli, H.: Effects of global ship emissions on European air pollution levels, *Atmos. Chem. Phys.*, 20, 11399–11422, <https://doi.org/10.5194/acp-20-11399-2020>, 2020.
- Kang, Y., Liu, M., Song, Y., Huang, X., Yao, H., Cai, X., Zhang, H., Kang, L., Liu, X., Yan, X., He, H., Zhang, Q., Shao, M., and Zhu, T.: High-resolution ammonia emissions inventories in China from 1980 to 2012, *Atmos. Chem. Phys.*, 16, 2043–2058, <https://doi.org/10.5194/acp-16-2043-2016>, 2016.
- Karjalainen, P., Teinila, K., Kuittinen, N., Aakko-Saksa, P., Bloss, M., Vesala, H., Pettinen, R., Saarikoski, S., Jalkanen, J. P., and Timonen, H.: Real-world particle emissions and secondary aerosol formation from a diesel oxidation catalyst and scrubber equipped ship operating with two fuels in a SECA area, *Environ. Pollut.*, 292, 118278, <https://doi.org/10.1016/j.envpol.2021.118278>, 2022.
- Kotchenruther, R. A.: The effects of marine vessel fuel sulfur regulations on ambient PM<sub>2.5</sub> along the west coast of the U.S., *Atmos. Environ.*, 103, 121–128, <https://doi.org/10.1016/j.atmosenv.2014.12.040>, 2015.
- Kotchenruther, R. A.: The effects of marine vessel fuel sulfur regulations on ambient PM<sub>2.5</sub> at coastal and near coastal monitoring sites in the U.S., *Atmos. Environ.*, 151, 52–61, <https://doi.org/10.1016/j.atmosenv.2016.12.012>, 2017.
- Lack, D. A., Corbett, J. J., Onasch, T., Lerner, B., Massoli, P., Quinn, P. K., Bates, T. S., Covert, D. S., Coffman, D., Sierau, B., Herndon, S., Allan, J., Baynard, T., Lovejoy, E., Ravishankara, A. R., and Williams, E.: Particulate emissions from commercial shipping: Chemical, physical, and optical properties, *J. Geophys. Res.*, 114, D00F04, <https://doi.org/10.1029/2008jd011300>, 2009.
- Lansø, A. S., Winther, M., Jensen, S. S., and Løfstrøm, P.: Impact on air quality from increasing cruise ship activity in Copenhagen port, *Environmental Research Communications*, 5, 021003, <https://doi.org/10.1088/2515-7620/acb90c>, 2023.
- Li, M., Zhang, Q., Kurokawa, J.-I., Woo, J.-H., He, K., Lu, Z., Ohara, T., Song, Y., Streets, D. G., Carmichael, G. R., Cheng, Y., Hong, C., Huo, H., Jiang, X., Kang, S., Liu, F., Su, H., and Zheng, B.: MIX: a mosaic Asian anthropogenic emission inventory under the international collaboration framework of the MICS-Asia and HTAP, *Atmos. Chem. Phys.*, 17, 935–963, <https://doi.org/10.5194/acp-17-935-2017>, 2017.
- Liu, H., Jin, X., Wu, L., Wang, X., Fu, M., Lv, Z., Morawska, L., Huang, F., and He, K.: The impact of marine shipping and its DECA control on air quality in the Pearl River Delta, China, *Sci. Total Environ.*, 625, 1476–1485, <https://doi.org/10.1016/j.scitotenv.2018.01.033>, 2018a.
- Liu, Y., Zhang, W., Bai, Z., Yang, W., Zhao, X., Han, B., and Wang, X.: China Source Profile Shared Service (CSPSS): The Chinese PM<sub>2.5</sub> Database for Source Profiles, *Aerosol Air Qual. Res.*, 17, 1501–1514, <https://doi.org/10.4209/aaqr.2016.10.0469>, 2017a.
- Liu, Y., Xing, J., Wang, S., Fu, X., and Zheng, H.: Source-specific speciation profiles of PM<sub>2.5</sub> for heavy metals and their anthropogenic emissions in China, *Environ. Pollut.*, 239, 544–553, <https://doi.org/10.1016/j.envpol.2018.04.047>, 2018b.
- Liu, Z., Lu, X., Feng, J., Fan, Q., Zhang, Y., and Yang, X.: Influence of Ship Emissions on Urban Air Quality: A Comprehensive Study Using Highly Time-Resolved Online Measurements and Numerical Simulation in Shanghai, *Environ. Sci. Technol.*, 51, 202–211, <https://doi.org/10.1021/acs.est.6b03834>, 2017b.
- Luo, Z., Lv, Z., Zhao, J., Sun, H., He, T., Yi, W., Zhang, Z., He, K., and Liu, H.: Shipping-related pollution decreased but mortality increased in Chinese port cities, *Nature Cities*, 1, 295–304, <https://doi.org/10.1038/s44284-024-00050-8>, 2024.
- Lv, Z., Liu, H., Ying, Q., Fu, M., Meng, Z., Wang, Y., Wei, W., Gong, H., and He, K.: Impacts of shipping emissions on PM<sub>2.5</sub>



- pollution in China, *Atmos. Chem. Phys.*, 18, 15811–15824, <https://doi.org/10.5194/acp-18-15811-2018>, 2018.
- Ma, M., Gao, Y., Ding, A., Su, H., Liao, H., Wang, S., Wang, X., Zhao, B., Zhang, S., Fu, P., Guenther, A. B., Wang, M., Li, S., Chu, B., Yao, X., and Gao, H.: Development and Assessment of a High-Resolution Biogenic Emission Inventory from Urban Green Spaces in China, *Environ. Sci. Technol.*, 56, 175–184, <https://doi.org/10.1021/acs.est.1c06170>, 2022.
- Ministry of Transport of the People's Republic of China: Report on China's Shipping Development in 2022, Ministry of Transport of the People's Republic of China, ISBN 978-7-114-18855-8, 2023 (in Chinese).
- Moldanová, J., Fridell, E., Popovicheva, O., Demirdjian, B., Tishkova, V., Faccinnetto, A., and Focsa, C.: Characterisation of particulate matter and gaseous emissions from a large ship diesel engine, *Atmos. Environ.*, 43, 2632–2641, <https://doi.org/10.1016/j.atmosenv.2009.02.008>, 2009.
- Moldanová, J., Fridell, E., Winnes, H., Holmin-Fridell, S., Boman, J., Jedynska, A., Tishkova, V., Demirdjian, B., Joulie, S., Bladt, H., Ivleva, N. P., and Niessner, R.: Physical and chemical characterisation of PM emissions from two ships operating in European Emission Control Areas, *Atmos. Meas. Tech.*, 6, 3577–3596, <https://doi.org/10.5194/amt-6-3577-2013>, 2013.
- Shang, F., Chen, D., Guo, X., Lang, J., Zhou, Y., Li, Y., and Fu, X.: Impact of Sea Breeze Circulation on the Transport of Ship Emissions in Tangshan Port, China, *Atmosphere*, 10, 723, <https://doi.org/10.3390/atmos10110723>, 2019.
- Sindelarova, K., Markova, J., Simpson, D., Huszar, P., Karlicky, J., Darras, S., and Granier, C.: Copernicus Atmosphere Monitoring Service Global Biogenic VOC emissions version 3.1 (CAMS-GLOB-BIOv3.1) [data set], <https://permalink.aeris-data.fr/CAMS-GLOB-BIO> (last access: 27 July 2023), 2021.
- Song, S.-K., Shon, Z.-H., Moon, S.-H., Lee, T.-H., Kim, H.-S., Kang, S.-H., Park, G.-H., and Yoo, E.-C.: Impact of international Maritime Organization 2020 sulfur content regulations on port air quality at international hub port, *J. Clean. Prod.*, 347, 131298, <https://doi.org/10.1016/j.jclepro.2022.131298>, 2022.
- Spada, N. J., Cheng, X., White, W. H., and Hyslop, N. P.: Decreasing Vanadium Footprint of Bunker Fuel Emissions, *Environ. Sci. Technol.*, 52, 11528–11534, <https://doi.org/10.1021/acs.est.8b02942>, 2018.
- Sun, J., Qin, M., Xie, X., Fu, W., Qin, Y., Sheng, L., Li, L., Li, J., Sulaymon, I. D., Jiang, L., Huang, L., Yu, X., and Hu, J.: Seasonal modeling analysis of nitrate formation pathways in Yangtze River Delta region, China, *Atmos. Chem. Phys.*, 22, 12629–12646, <https://doi.org/10.5194/acp-22-12629-2022>, 2022.
- Tang, L., Ramacher, M. O. P., Moldanová, J., Matthias, V., Karl, M., Johansson, L., Jalkanen, J.-P., Yaramenka, K., Aulinger, A., and Gustafsson, M.: The impact of ship emissions on air quality and human health in the Gothenburg area – Part 1: 2012 emissions, *Atmos. Chem. Phys.*, 20, 7509–7530, <https://doi.org/10.5194/acp-20-7509-2020>, 2020.
- Tao, L., Fairley, D., Kleeman, M. J., and Harley, R. A.: Effects of switching to lower sulfur marine fuel oil on air quality in the San Francisco Bay area, *Environ. Sci. Technol.*, 47, 10171–10178, <https://doi.org/10.1021/es401049x>, 2013.
- UNCTAD: Review of Maritime Transport 2023: Towards a Green and Just Transition, in: United Nations Conference on Trade and Development (UNCTAD), United Nations Publications, Geneva, Switzerland, ISBN 978-92-1-002886-8, 2023.
- Viana, M., Hammings, P., Colette, A., Querol, X., Degraeuwe, B., Vlieger, I. d., and van Aardenne, J.: Impact of maritime transport emissions on coastal air quality in Europe, *Atmos. Environ.*, 90, 96–105, <https://doi.org/10.1016/j.atmosenv.2014.03.046>, 2014.
- Wang, G., Tao, Y., Chen, J., Liu, C., Qin, X., Li, H., Yun, L., Zhang, M., Zheng, H., Gui, H., Liu, J., Huo, J., Fu, Q., Deng, C., and Huang, K.: Quantitative Decomposition of Influencing Factors to Aerosol pH Variation over the Coasts of the South China Sea, East China Sea, and Bohai Sea, *Environ. Sci. Technol. Lett.*, 9, 815–821, <https://doi.org/10.1021/acs.estlett.2c00527>, 2022.
- Wang, X., Shen, Y., Lin, Y., Pan, J., Zhang, Y., Louie, P. K. K., Li, M., and Fu, Q.: Atmospheric pollution from ships and its impact on local air quality at a port site in Shanghai, *Atmos. Chem. Phys.*, 19, 6315–6330, <https://doi.org/10.5194/acp-19-6315-2019>, 2019.
- Wang, X., Yi, W., Lv, Z., Deng, F., Zheng, S., Xu, H., Zhao, J., Liu, H., and He, K.: Ship emissions around China under gradually promoted control policies from 2016 to 2019, *Atmos. Chem. Phys.*, 21, 13835–13853, <https://doi.org/10.5194/acp-21-13835-2021>, 2021.
- Wang, X., Liu, H., Zhang, J., Fu, X., Chen, D., Zhang, W., Yi, W., Lv, Z., Zhang, Q., and He, K.: Global shipping emissions from 1970 to 2021: Structural and spatial change driven by trade dynamics, *One Earth*, 10, 101243, <https://doi.org/10.1016/j.oneear.2025.101243>, 2025.
- WHO: WHO global air quality guidelines. Particulate matter (PM<sub>2.5</sub> and PM<sub>10</sub>), ozone, nitrogen dioxide, sulfur dioxide and carbon monoxide, Bonn, Germany, ISBN 978-92-4-003421-1, 2021.
- Xie, X., Hu, J., Qin, M., Guo, S., Hu, M., Wang, H., Lou, S., Li, J., Sun, J., Li, X., Sheng, L., Zhu, J., Chen, G., Yin, J., Fu, W., Huang, C., and Zhang, Y.: Modeling particulate nitrate in China: Current findings and future directions, *Environ. Int.*, 166, 107369, <https://doi.org/10.1016/j.envint.2022.107369>, 2022.
- Yang, L., Zhang, Q., Zhang, Y., Lv, Z., Wu, L., and Mao, H.: Real-world emission characteristics of an ocean-going vessel through long sailing measurement, *Sci. Total Environ.*, 810, 152276, <https://doi.org/10.1016/j.scitotenv.2021.152276>, 2022.
- Yi, W., Wang, X., He, T., Liu, H., Luo, Z., Lv, Z., and He, K.: The high-resolution global shipping emission inventory by the Shipping Emission Inventory Model (SEIM), *Earth Syst. Sci. Data*, 17, 277–292, <https://doi.org/10.5194/essd-17-277-2025>, 2025.
- Yu, G., Zhang, Y., Yang, F., He, B., Zhang, C., Zou, Z., Yang, X., Li, N., and Chen, J.: Dynamic Ni/V Ratio in the Ship-Emitted Particles Driven by Multiphase Fuel Oil Regulations in Coastal China, *Environ. Sci. Technol.*, 55, 15031–15039, <https://doi.org/10.1021/acs.est.1c02612>, 2021.
- Zetterdahl, M., Moldanová, J., Pei, X., Pathak, R. K., and Demirdjian, B.: Impact of the 0.1 % fuel sulfur content limit in SECA on particle and gaseous emissions from marine vessels, *Atmos. Environ.*, 145, 338–345, <https://doi.org/10.1016/j.atmosenv.2016.09.022>, 2016.
- Zhai, J., Yu, G., Zhang, J., Shi, S., Yuan, Y., Jiang, S., Xing, C., Cai, B., Zeng, Y., Wang, Y., Zhang, A., Zhang, Y., Fu, T. M., Zhu, L., Shen, H., Ye, J., Wang, C., Tao, S., Li, M., Zhang, Y., and Yang, X.: Impact of Ship Emissions on Air Quality in the Greater Bay Area in China under the Latest Global Ma-

- rine Fuel Regulation, *Environ. Sci. Technol.*, 57, 12341–12350, <https://doi.org/10.1021/acs.est.3c03950>, 2023.
- Zhang, F., Xiao, B., Liu, Z., Zhang, Y., Tian, C., Li, R., Wu, C., Lei, Y., Zhang, S., Wan, X., Chen, Y., Han, Y., Cui, M., Huang, C., Wang, H., Chen, Y., and Wang, G.: Real-world emission characteristics of VOCs from typical cargo ships and their potential contributions to secondary organic aerosol and O<sub>3</sub> under low-sulfur fuel policies, *Atmos. Chem. Phys.*, 24, 8999–9017, <https://doi.org/10.5194/acp-24-8999-2024>, 2024.
- Zhang, X., Zhang, Y., Liu, Y., Zhao, J., Zhou, Y., Wang, X., Yang, X., Zou, Z., Zhang, C., Fu, Q., Xu, J., Gao, W., Li, N., and Chen, J.: Changes in the SO<sub>2</sub> Level and PM<sub>2.5</sub> Components in Shanghai Driven by Implementing the Ship Emission Control Policy, *Environ. Sci. Technol.*, 53, 11580–11587, <https://doi.org/10.1021/acs.est.9b03315>, 2019a.
- Zhang, Y., Deng, F., Man, H., Fu, M., Lv, Z., Xiao, Q., Jin, X., Liu, S., He, K., and Liu, H.: Compliance and port air quality features with respect to ship fuel switching regulation: a field observation campaign, SEISO-Bohai, *Atmos. Chem. Phys.*, 19, 4899–4916, <https://doi.org/10.5194/acp-19-4899-2019>, 2019b.
- Zhao, J., Zhang, Y., Xu, H., Tao, S., Wang, R., Yu, Q., Chen, Y., Zou, Z., and Ma, W.: Trace Elements From Ocean-Going Vessels in East Asia: Vanadium and Nickel Emissions and Their Impacts on Air Quality, *J. Geophys. Res.-Atmos.*, 126, e2020JD033984, <https://doi.org/10.1029/2020jd033984>, 2021.
- Zhao, M., Zhang, Y., Ma, W., Fu, Q., Yang, X., Li, C., Zhou, B., Yu, Q., and Chen, L.: Characteristics and ship traffic source identification of air pollutants in China's largest port, *Atmos. Environ.*, 64, 277–286, <https://doi.org/10.1016/j.atmosenv.2012.10.007>, 2013.
- Zheng, B., Zhang, Q., Geng, G., Chen, C., Shi, Q., Cui, M., Lei, Y., and He, K.: Changes in China's anthropogenic emissions and air quality during the COVID-19 pandemic in 2020, *Earth Syst. Sci. Data*, 13, 2895–2907, <https://doi.org/10.5194/essd-13-2895-2021>, 2021.
- Zheng, H., Cai, S., Wang, S., Zhao, B., Chang, X., and Hao, J.: Development of a unit-based industrial emission inventory in the Beijing–Tianjin–Hebei region and resulting improvement in air quality modeling, *Atmos. Chem. Phys.*, 19, 3447–3462, <https://doi.org/10.5194/acp-19-3447-2019>, 2019.